TKK Dissertations 248
Espoo 2010

DYNAMIC STRAIN AGING OF AUSTENITIC STAINLESS STEELS AND Ni-BASE ALLOYS

Doctoral Dissertation

Mykola Ivanchenko

Aalto University
School of Science and Technology
Faculty of Engineering and Architecture
Department of Engineering Design and Production

TKK Dissertations 248
Espoo 2010

DYNAMIC STRAIN AGING OF AUSTENITIC STAINLESS STEELS AND Ni-BASE ALLOYS

Doctoral Dissertation

Mykola Ivanchenko

Doctoral dissertation for the degree of Doctor of Science in Technology to be presented with due permission of the Faculty of Engineering and Architecture for public examination and debate in Auditorium K216 at the Aalto University School of Science and Technology (Espoo, Finland) on the 19th of November 2010 at 12 noon.

Aalto University
School of Science and Technology
Faculty of Engineering and Architecture
Department of Engineering Design and Production

Aalto-yliopisto
Teknillinen korkeakoulu
Insinööritieteiden ja arkkitehtuurin tiedekunta
Koneenrakennustekniikan laitos

Distribution:
Aalto University
School of Science and Technology
Faculty of Engineering and Architecture
Department of Engineering Design and Production
P.O. Box 14200 (Puumiehenkuja 3 A)
FI - 00076 Aalto
FINLAND
URL: http://edp.tkk.fi/en/
Tel. +358-9-470 23538
Fax +358-9-470 23537
E-mail: johanna.salmela@tkk.fi

ISBN 978-952-60-3444-7
ISBN 978-952-60-3445-4 (PDF)
ISSN 1795-2239
ISSN 1795-4584 (PDF)
URL: http://lib.tkk.fi/Diss/2010/isbn9789526034454/

TKK-DISS-2832

Yliopistopaino
Helsinki 2010

Aalto University

ABSTRACT OF DOCTORAL DISSERTATION	AALTO UNIVERSITY SCHOOL OF SCIENCE AND TECHNOLOGY P.O. BOX 11000, FI-00076 AALTO http://www.aalto.fi

Author Mykola Ivanchenko

Name of the dissertation
Dynamic strain aging of austenitic stainless steels and Ni-base alloys

Manuscript submitted 04.06.2010	Manuscript revised 22.09.2010

Date of the defence 19.11.2010

☐ Monograph ☒ Article dissertation (summary + original articles)

Faculty Faculty of Engineering and Architecture
Department Department of Engineering Design and Production
Field of research Engineering Materials
Opponent(s) Prof. David Delafosse and Prof. Tuomo Tiainen
Supervisor Prof. Hannu Hänninen
Instructor Dr. Yuriy Yagodzinskyy

Abstract

Dynamic strain aging (DSA) affects mechanical properties of materials and promotes strain localization. DSA results in serrated plastic flow, which was observed by means of constant extension rate tensile (CERT) tests in different grades of AISI 316 austenitic stainless steel and Ni-base alloys Alloy 600 and Alloy 690 in the temperature range of 200 – 600 ^{o}C and values of strain rate from 10^{-6} to 10^{-3} s^{-1}. Negative strain rate sensitivity was reported for the studied materials at temperatures and strain rates where serrated plastic flow appeared. The map for the occurrence of serrated flow as a function of strain rate and temperature was built for the materials. The activation enthalpies of dynamic strain aging appearance were found to be 120 kJ/mol for the austenitic stainless steel and 159 kJ/mol for both Ni-base alloys. The internal friction (IF) peak associated with the interstitial atoms of nitrogen and carbon in the solid solution of AISI 316NG austenitic stainless steel and Alloy 600 was reported. The activation enthalpies of nitrogen diffusion in AISI 316NG steel (140 kJ/mol) and carbon diffusion in Alloy 600 (162 kJ/mol), obtained by means of internal friction, correspond well to the activation enthalpies of DSA appearance. The height of the internal friction peak increases depending on the pre-straining conditions in the similar way for AISI 316NG steel and Alloy 600. Annealing in situ at the IF peak temperature results in the decay of the IF peak enhanced by pre-straining for both materials. At the initial stage, the peak annealing processes can be described as an exponential decay function with characteristic times of 0.95 and 0.92 ks for AISI 316NG steel and Alloy 600, respectively. Transmission electron microscopy was performed on the specimens of AISI 316NG steel after CERT tests at temperatures of 400 and 200 ^{o}C, where serrated and smooth plastic flow was observed, respectively. Long-range planarity was observed in the dislocation structures of the specimen tested at 400 ^{o}C. The microstructure of the specimen strained at 200 ^{o}C exhibited cellular dislocation structure. It was concluded, that the diffusive re-distribution of interstitial atoms in the DSA regime affected the deformation behavior of the material by restricting dislocation cross-slip, which in turn promotes strain localization, affecting the mechanical performance of the material.

Keywords Dynamic strain aging, austenitic stainless steel, Ni-base alloy, mechanical spectroscopy, TEM

ISBN (printed) 978-952-60-3444-7	ISSN (printed) 1795-2239
ISBN (pdf) 978-952-60-3445-4	ISSN (pdf) 1795-4584
Language English	Number of pages 90 p. + app. 38 p.

Publisher Aalto University, Department of Engineering Design and Production

Print distribution Aalto University, Dep. of Engineering Design and Production, Lab. of Engineering Materials

☒ The dissertation can be read at http://lib.tkk.fi/Diss/2010/isbn9789526034454/

Aalto University

VÄITÖSKIRJAN TIIVISTELMÄ	AALTO-YLIOPISTO TEKNILLINEN KORKEAKOULU PL 11000, 00076 AALTO http://www.aalto.fi
Tekijä Mykola Ivanchenko	
Väitöskirjan nimi Austeniittisten ruostumattomien terästen ja Ni-seosten dynaaminen myötövanheneminen	
Käsikirjoituksen päivämäärä 04.06.2010	Korjatun käsikirjoituksen päivämäärä 22.09.2010
Väitöstilaisuuden ajankohta 19.11.2010	
☐ Monografia	☒ Yhdistelmäväitöskirja (yhteenveto + erillisartikkelit)
Tiedekunta Insinööritieteiden ja arkkitehtuurin tiedekunta Laitos Koneenrakennustekniikan laitos Tutkimusala Materiaalitekniikka Vastaväittäjä(t) Prof. David Delafosse and Prof. Tuomo Tiainen Työn valvoja Prof. Hannu Hänninen Työn ohjaaja TkT Yuriy Yagodzinskyy	

Tiivistelmä

Dynaaminen myötövanheneminen (Dynamic Strain Aging, DSA) vaikuttaa materiaalin mekaanisiin ominaisuuksiin ja suosii muodonmuutoksen paikallistumista. DSA johtaa sahalaitaiseen plastiseen muodonmuutokseen, joka havaittiin (Constant Extension Rate Tensile, CERT) kokeissa AISI 316 ruostumattomassa teräksessä ja Ni-seoksissa Alloy 600 ja Alloy 690 lämpötila-alueella 200 – 600 ^{o}C muodonmuutosnopeuksilla 10^{-6} … 10^{-3} s^{-1}. Tutkituilla materiaaleilla havaittiin negatiivinen m-eksponentti (strain rate sensitivity factor) lämpötiloissa ja muodonmuutosnopeuksilla, joissa tapahtui sahalaitaista plastista muodonmuutosta. Materiaaleille tehtiin kartta sahalaitaisen muodonmuutoksen esiintymiselle muodonmuutosnopeuden ja lämpötilan funktiona. Dynaamisen myötövanhenemisen aktivaatioenergiat olivat ruostumattomalle teräkselle 120 kJ/mol ja Ni-seoksille 159 kJ/mol. Sisäisen kitkan (Internal Friction, IF) mittausten avulla saatiin typen diffuusion aktivaatioenergiaksi AISI 316NG-teräksellä 140 kJ/mol ja hiilen diffuusiolle Alloy 600-seoksella 162 kJ/mol. Nämä vastaavat hyvin DSA:n esiintymisen aktivaatioenergioita. Sisäisen kitkan piikin korkeus kasvaa muokkauksen vaikutuksesta samalla tavalla AISI 316NG-teräksellä ja Alloy 600-seoksella. Sisäinen kitkan piikin lämpötilassa tapahtuva hehkutus johtaa muokkauksen vaikutuksen pienenemiseen molemmissa materiaaleissa. Alkuvaiheessa piikin pieneneminen voidaan kuvata eksponentiaalifunktiolla, jonka ominaiskerroin on 0,95 ks AISI 316NG-teräksellä ja 0,92 ks Alloy 600-seoksella. AISI 316NG-teräsnäytteet tutkittiin läpivalaisuelektronimikroskoopilla lämpötiloissa 400 ja 200 ^{o}C suoritettujen CERT – kokeiden jälkeen, joissa havaittiin vastaavasti sahalaitainen ja tasainen plastinen muodonmuutos. Pitkänmatkan tasomainen dislokaatiorakenne havaittiin 400 ^{o}C:ssa testatussa näytteessä. 200 ^{o}C:ssa testatun näytteen dislokaatiorakenne oli sellimäinen. Tulosten perusteella pääteltiin, että diffuusion avulla tapahtuva välisija-atominen uudelleen jakautuminen DSA-olosuhteissa vaikutti materiaalin deformaatiokäyttäytymiseen estämällä dislokaatioiden ristiliukumisen. Tämä edisti deformaation paikallistumista ja huononsi materiaalin mekaanisia ominaisuuksia.

Asiasanat Dynaaminen myötövanheneminen, austeniittinen ruostumaton teräs, Ni-seos, mekaaninen spektroskopia, läpivalaisuelektronimikroskopia	
ISBN (painettu) 978-952-60-3444-7	ISSN (painettu) 1795-2239
ISBN (pdf) 978-952-60-3445-4	ISSN (pdf) 1795-4584
Kieli Englanti	Sivumäärä 90 s. + liit. 38 p.
Julkaisija Aalto-yliopisto, Koneenrakennustekniikan laitos	
Painetun väitöskirjan jakelu Aalto-yliopisto, Koneenrakennustekniikan laitos, Materiaalitekniikka	
☒ Luettavissa verkossa osoitteessa http://lib.tkk.fi/Diss/2010/isbn9789526034454/	

Preface

Present research work was carried out in the Laboratory of Engineering Materials at Aalto University School of Science and Technology (former Helsinki University of Technology (HUT)). This work was initiated in cooperation with VTT Technical Research Centre of Finland within the project on structural operability and plant life management (RKK and XVO). At the initial stage, the funding has been provided by Centre for International Mobility (CIMO), which is gratefully acknowledged. It is impossible to overestimate the importance of the membership in post-graduate program of the "Graduate School on New Materials and Processes" sponsored by Academy of Finland during the years 2006 – 2009, which made possible to concentrate to the post-graduate studies and writing the scientific journal publications and also gave me an opportunity to get acquainted with Finnish industry and to participate lectures from world known specialists in the field of materials science. At the final stage this work was also partly funded from SAFIR 2010 funded by VYR (State Waste Management Fund), VTT (Technical Research Centre of Finland), the Swedish Radiation Safety Authority, the National Technology Agency (Tekes), TVO, Fortum, Neste, Vattenfall, OKG and Metso.

I wish to express my gratitude to my supervisor, Prof. Hannu Hänninen, for the opportunity to do my doctoral thesis in the laboratory, for his patient guidance, encouragement and valuable ideas and comments on my work. I am also grateful to Dr. Yuriy Yagodzinskyy, who has taught me the scientific way of thinking, shared with me his enormous scientific experience and knowledge and was my mentor for the time of my work in the laboratory. It is my pleasure to acknowledge the collaboration with the whole personnel of the Laboratory of Engineering Materials, which created a pleasant working environment. My special thanks go to Kim Widell for the assistance with the experiments, Risto Ilola for my supervision in the graduate school, Vitaliy Nevdacha for teaching me the basics of internal friction measurements and Jyrki Romu for general assistance. Finally, I would like to thank my family and friends for their support. My

special thanks I wish to send to my dear Svetlana and our son Timofey for brining lots of happy moments into my life, for their love and patience.

Espoo, September 2010

Mykola Ivanchenko

Contents

Research hypothesis and original features

As the hypothesis, it is supposed that the redistribution of interstitials in austenitic stainless steels and Ni-base alloys loaded under the dynamic strain aging conditions at the corresponding temperatures, leads to concentration inhomogeneities of interstitial atoms in submicron-size characteristic scale, which may restrict cross-slip and lead to the formation of strain localization, which can result in crack nucleation. Deformation of the materials under DSA conditions undergoes with variation of the strain rate in time and space by large factors, which results in a higher crack initiation rate. Deformation under the DSA conditions affects also crack tip plasticity and causes localization of strain and in this way enhances crack propagation rate. It is believed that the formation of strain localization together with the variation of strain rate and the changes in crack tip plasticity lead to the enhancement of environment assisted cracking.

The following features are believed to be original:

1. In austenitic stainless steel grade 316 and Ni-base Alloys 600 and 690, dynamic strain aging, which is manifested by serrated plastic flow and negative strain rate sensitivity at temperatures around 300 ^{o}C and strain rates in the range of 10^{-6} – 10^{-4} s^{-1}, is caused by the interaction of mobile dislocations with interstitial atoms, such as nitrogen and carbon.

2. The internal friction peak observed in Ni-base Alloy 600 in the range of temperatures from 300 to 400 ^{o}C is attributed to Snoek-like relaxation caused by the presence of free carbon interstitial atoms in the lattice of alloy.

3. Plastic deformation by straining at elevated temperatures results in an increase in the amplitude of nitrogen-/carbon-induced Snoek-like IF peak in 316NG austenitic SS and Ni-base Alloy 600. Increase in the peak amplitude becomes remarkable after pre-straining under the DSA conditions, which evidences similar origins of the Snoek-like peak evolution with prior deformation under

the DSA conditions in both AISI 316NG austenitic stainless steel and Ni-base Alloy 600.

4. Deformation of 316NG austenitic stainless steel under dynamic strain aging conditions results in the long range planarity of dislocation structure, which, in turn, promotes strain localization.

5. Cold work of austenitic stainless steel results in the internal friction peak with two well-defined components, which depend on the amount of plastic deformation. The low-temperature component of the observed peak has relaxation origin with similar characteristics of Hasiguti peaks and, thus, is assumed to represent dislocation-point defect interactions. The high-temperature component of the studied peak is transitional IF peak, which is related to the annihilation of vacancies, which are presumably formed during the plastic deformation, and to their diffusion to the dislocation cores.

List of Publications

This thesis consists of an overview and of the following publications which are referred to in the text by their Roman numerals.

I Ivanchenko, M., Ehrnstén, U., Nevadacha, V., Yagodzinskyy, Y. and Hänninen, H. Dynamic strain ageing of nitrogen-alloyed AISI 316L stainless steel. In: N. Akdut, B.C. De Cooman, J. Foct (eds.). Proceedings of the 7th International Conference on High Nitrogen Steels 2004. Ostend, Belgium, 19-22.09.2004. GRIPS' Sparkling World of Steel Vol. 1: Proceedings, No. 4. pp. 641 - 649.

II Ehrnstén, U., Ivanchenko, M., Nevdacha, V., Yagodzinskyy, Y., Toivonen, A. and Hänninen, H. Dynamic strain ageing and EAC of deformed nitrogen-alloyed AISI 316 stainless steels. In: T.R. Allen, P.J. King, L. Nelson (eds.). Proceedings of the 12th International Conference on Environmental Degradation of Materials in Nuclear Power System – Water Reactors, 2005. Salt Lake City, Utah, USA, 14-18.8.2005. TMS. pp. 1475-1482.

III Karlsen, W., Ivanchenko, M., Ehrnstén, U., Yagodzinskyy Y. and Hanninen, H. Microstructural manifestation of dynamic strain aging in AISI 316 stainless steel. Journal of Nuclear Materials, 2009. Vol. 395:1-3. pp. 156-161.

IV Ivanchenko, M., Yagodzinskyy, Y. and Hänninen, H. Effect of plastic deformation on anelastic mechanical losses in multicomponent substitutional austenitic alloys. Material Science and Engineering A, 2008. Vol. 521-522. pp. 121-123.

V Hänninen, H., Ivanchenko, M., Yagodzinskyy, Y., Nevdacha, V., Ehrnstén, U. and Aaltonen, P. Dynamic strain aging of Ni-base alloys Inconel 600 and 690. In: T.R. Allen, P.J. King, L. Nelson (eds.). Proceedings of the 12th International Conference on Environmental Degradation of Materials in Nuclear Power System – Water Reactors, 2005. Salt Lake City, Utah, USA, 14-18.8.2005. TMS. pp. 1423-1430.

VI Ivanchenko, M., Nevdacha, V., Yagodzinskyy, Y. and Hänninen, H. Internal friction studies of carbon and its redistribution kinetics in Inconel 600 and 690 alloys under dynamic strain aging conditions. Material Science and Engineering A, 2006. Vol. 442:1-2. pp. 458-461.

Author's contribution

Present thesis consists of six original publications and an introductory part. The objects of the research were commercial (316NG austenitic stainless steel and Ni-base alloys Inconel® Alloy 600 and Alloy 690) and some model alloys (nitrogen-alloyed 316L austenitic stainless steels). The introductory part aims to provide the state-of-the-art in the research field of dynamic strain aging and its possible effects on environment assisted cracking. It also aims to answer the question of possibilities to study interstitial distribution, in particular carbon and nitrogen, by method of internal friction (or mechanical spectroscopy) in multicomponent alloys with face-centred-cubic lattice. The similarities and differences in the redistribution of interstitials in austenitic stainless steels (particularly in 316NG) and commercial Ni-base alloys (Inconel® Alloy 600 and Alloy 690) are studied.

The research work presented in listed publications was mainly done in the Laboratory of Engineering Materials at Aalto University School of Science and Technology. Part of the results was obtained in the Technical Research Centre of Finland VTT.

In **Publication I** dynamic strain aging (DSA) of nitrogen-alloyed 316 L stainless steels with three different contents of nitrogen and a commercial 316NG steel designed for nuclear industry applications was investigated by means of slow strain rate tensile tests. Tensile tests were performed at three different strain rates, 10^{-4}, 10^{-5} and 5×10^{-6} s^{-1}, in the range of temperatures of 200 to 400 ^{o}C. It has been found that DSA in studied stainless steels occurs at temperatures below 300 ^{o}C, when the strain rate is less than 10^{-4} s^{-1}. It was also observed that nitrogen alloying suppresses the serrated flow development in studied steels and shifts its occurrence to higher temperatures. Fourier analysis of the stress serration was performed and an average time between the stress pulses was estimated to be 2.83 ks. The presence of free nitrogen in the steel lattice and its diffusion parameters were studied by using low-frequency internal friction method. Activation enthalpy of DSA appearance in 316NG steel obtained from the strain rate –

temperature map of DSA was found to be 120 kJ/mol, which is close to 140 kJ/mol for the activation enthalpy of nitrogen diffusion in 316NG steel.

In this article the author has run all the tensile tests, prepared samples for the tensile tests and internal friction measurements and processed all the obtained results, except of internal friction measurements. Vitaliy Nevdacha has ran the internal friction measurements and Ulla Ehrnstén has supplied the bulk materials for the study, provided chemical analyses of the studied steels and participated in the discussion of the results. Writing was a joint effort of Mykola Ivanchenko, Yuriy Yagodzinskyy and Hannu Hänninen.

Publication II. The effect of cold work and nitrogen content on the deformation behaviour of austenitic stainless steels was investigated. The materials were austenitic stainless steels of AISI 316L type with different amounts of nitrogen (0.03…0.18%) and they were deformed in tension 0, 5 and 20% before further investigations. The investigations were focused on the dynamic strain ageing (DSA) behaviour as a function of nitrogen level and deformation. A few crack growth rate measurements were performed on nuclear grade AISI 316NG stainless steel with different degrees of deformation (0, 5 and 20%). The effects of DSA on mechanical properties of these materials were evaluated based on the peaks in tensile strength and minimum in ductility in the DSA temperature range. The strain rate sensitivity in the DSA temperature range was also investigated. Internal friction measurements were performed in the temperature range of -100…600 ^{o}C for determining nitrogen interactions with other alloying elements and dislocations. The results show effects of nitrogen on the stainless steel deformation behaviour, i.e. clear indications of dynamic strain ageing: serrated yielding, negative strain rate sensitivity and changes in the internal friction behaviour as a function of nitrogen content and amount of deformation. The apparent activation energy calculated from the DSA serration occurrence map corresponds to that of nitrogen diffusion. Fully intergranular cracking was obtained in the 20% deformed, non-sensitised 316NG stainless steel in simulated BWR environment.

The author was responsible for the performance of the stepwise tensile tests for the evaluation of strain rate sensitivity and calculation of mechanical properties. Hardness measurements and microstructural characterisation of the studied steels were performed at VTT under supervision of Ulla Ehrnstén. Crack growth rate measurements on nuclear grade AISI 316NG stainless steel with different degrees of cold work were performed by Aki Toivonen. Writing of the article was a joint effort of the co-authors.

Publication III. In the current study, the deformation microstructures of AISI 316 stainless steel specimens were examined after tensile testing at several temperatures both in and out of the DSA-region (200, 288 and 400 ^{o}C), and the effect of straining on free nitrogen evolution at those temperatures was studied by Anelastic Mechanical Loss Spectrometry (Internal Friction). Analysis of the nitrogen-induced Snoek-like peak after straining indicated that DSA behaviour is associated with the formation of sub-micron scale nitrogen-enriched zones in the austenitic matrix. Long-range planarity was observed in the dislocation structures at 400 ^{o}C and short-range planarity at 288 ^{o}C, but at 200 ^{o}C the microstructure exhibited cellular dislocation structure. Diffusion re-distribution of nitrogen in the DSA-regime affected the deformation behaviour of the material by restricting cross-slip, which in turn promotes strain localization and affects the mechanical performance of the material.

This publication was mainly written by the author and Wade Karlsen, who has also performed, analysed and discussed results related to transmission electron microscopy, while the author has run and discussed all the results obtained by tensile tests and internal friction measurements. Yuriy Yagodzinskyy has contributed to this article through his valuable comments and suggestions in the interpretation of the results. The work was coordinated by Ulla Ehrnstén and Hannu Hänninen, who also provided valuable comments, which improved the quality of the publication.

Publication IV. Complex two-component peak of anelastic mechanical losses was observed in multicomponent substitutional austenitic alloys after prior plastic deformation. In AISI 316L, AISI 316LN, AISI 310 and AISI 304 austenitic stainless

steels, this peak is located in a wide range of temperatures from 200 to 400 K. Characteristics of the observed peak for different thermo-mechanical treatments were studied employing low-carbon AISI 316L austenitic stainless steel. It is shown that the low-temperature component (peak P1 with maximum at 250 K) has a relaxation origin, while the high-temperature component (peak P2 located at 340-360 K) represents a transitional process developing in a deformed austenitic stainless steel during linear heating. The activation enthalpy and the pre-exponential factor of the relaxation time of peak P1 are 46 ± 5.8 kJ/mol and $10^{-11\pm1}$ s, respectively. Effects of prior cold deformation and heating rate on the observed anelastic mechanical losses are also described. The origins of the peaks are discussed in terms of interactions of dislocations with point defects generated by plastic deformation.

In this article all the experimental part and writing was done by the author. Interpretation of the obtained results was greatly assisted by Yuriy Yagodzinskyy together with Hannu Hänninen who provided valuable comments that substantially improved the technical quality of the paper.

Publication V. Dynamic strain aging (DSA) and jerky flow phenomena in the commercial Ni-base alloys Inconel® Alloy 600 and Alloy 690 have been investigated. Tensile tests were performed in the strain rate range of 10^{-3} to 10^{-6} s^{-1} at temperatures of 100 – 600 ^{o}C. No remarkable difference in the DSA behaviour of Alloy 600 and Alloy 690 was observed. Tensile properties of the studied alloys in the DSA temperature range, and type and characteristics of jerky flow were obtained and analysed. The map for the occurrence of serrated flow as a function of strain rate and temperature was built for Alloy 600 and Alloy 690 alloys and the activation enthalpies of dynamic strain aging appearance were found to be ~160 kJ/mol for both materials. The obtained enthalpy of DSA appearance corresponds well to the enthalpy of carbon diffusion (~170 kJ/mol), which was estimated by means of internal friction for the studied Alloy 600. The mechanisms of DSA based on interstitial atom interactions with dislocations in the studied alloys are discussed and the results are analysed based on the susceptibility of these alloys to environment assisted cracking (EAC).

The author has run all the tensile tests, prepared samples for the tensile tests and internal friction measurements and processed all the obtained results, except the internal friction measurements which were performed by Vitaliy Nevdacha. Ulla Ehrnstén and P. Aaltonen have provided the bulk materials for the study, provided chemical analyses of the studied alloys and participated in the discussion of the results. Writing was a joint effort of Mykola Ivanchenko, Yuriy Yagodzinskyy and Hannu Hänninen.

Publication VI. Carbon Snoek-like relaxation peak with a height of about 10^{-4} was found in annealed Ni-base Alloy 600 at 620 – 670 K while no carbon-induced peaks were observed in Alloy 690. The activation enthalpy and the pre-exponential factor of the relaxation time were refined as 162 ± 8.7 kJ/mol and $10^{-14.14 \pm 0.72}$ s, respectively. The height of the observed peak increases dramatically, up to about 10^{-3}, after tensile deformation of Alloy 600 at 423 K at the strain rate of 10^{-5} s^{-1}, when dynamic strain aging (DSA) behavior exhibits well developed serrations on the tensile stress-strain curve. Annealing *in situ* at the carbon peak temperature results in decay of the peak amplitude, which consists of two exponential stages with characteristic times of 1.6 ks and 21.9 ks, respectively. The first characteristic time is in good agreement with the mean period of DSA serrations. The second characteristic time can be related to depletion of free carbon concentration due to carbide growth or to segregation of carbon to grain boundaries.

The author analyzed results obtained by means of internal friction with assistance of Vitaliy Nevdacha, and has performed major writing of the article together with Yuriy Yagodzinskyy, who has actively contributed to the discussion part. The work has been performed under supervision of Hannu Hänninen, who has participated in revision of the manuscript.

List of Abbreviations

BWR	Boiling water reactor
BCC	Body-centred cubic lattice
CERT	Constant elongation rate tensile test
DSA	Dynamic strain aging
EAC	Environment assisted cracking
FFT	Fast Fourier transformation
FCC	Face-centred cubic lattice
HAZ	Heat affected zone
HR	Heating rate
IF	Internal friction
IGSCC	Intergranular stress corrosion cracking
PLC	Portevin-Le Chatelier effect
PWR	Pressurised water reactor
RT	Room temperature
SCC	Stress corrosion cracking
SS	Stainless steel
SSRT	Slow strain rate tensile test
SRS	Strain rate sensitivity
TEM	Transmission electron microscopy
UTS	Ultimate tensile stress
YS	Yield stress

List of Symbols

b	Burgers vector
C_1	Solute concentration at the dislocation core which is required to lock it
C_0	Solute concentration of the alloy
C_v	Vacancy concentration
D	Diffusion coefficient
D_0	Diffusion frequency factor
E	Elastic modulus
J	Modulus of compliance
H	Effective activation enthalpy (or apparent activation energy)
k_B	Boltzmann's constant
L	Average distance between arresting obstacles
M	Modulus of elasticity
Q_m	Activation energy for solute migration
Q^{-1}	Internal friction
T	Temperature
T_m	Temperature of an internal friction peak maximum
t_a	Aging time
t_w	Waiting time
U_m	Binding energy of solute atom to dislocation
W	Maximum stored elastic energy per cycle of loading
ΔW	Energy absorption per cycle of loading
Δ	Relaxation strength

ε	Strain
ε_c	Critical strain to initiate DSA
$\dot{\varepsilon}$	Strain rate
σ	Stress
ϕ	Loss angle
ψ	Specific damping capacity
ρ_m	Density of mobile dislocations
τ	Relaxation time
τ_0	Limit relaxation time (or pre-exponential factor of the relaxation time)
$\bar{v}$	Average velocity of dislocations
ω	Circular frequency

Subscripts

p	Plastic
e	Elastic
R	Relaxed value
U	Unrelaxed value

1 Introduction

Since the early 1970´s numerous cases of intergranular stress corrosion cracking (IGSCC) have occurred in boiling water reactors (BWR) in 304 type austenitic stainless steels. The root cause for the cracking is a combination of tensile stresses, an oxidising environment and a sensitised material. The remedial actions taken have involved all three major parameters, e.g. application of narrow-gap welding technique to reduce residual stresses, increase of the overall purity of the primary water, application of hydrogen or noble metal water chemistry as well as the reduction of the amount of carbon in the stainless steels to avoid sensitisation. Nitrogen is added to maintain the strength level of austenitic stainless steels with reduced carbon levels. The remedial actions have been successful and the amount of cracking due to IGSCC has decreased remarkably. However, in the early 90´s the first cases of intergranular (IG) stress corrosion cracking in non-sensitised, low carbon austenitic stainless steels of type 316NG and 304L were observed (Angeliu, 2001; Ehrnstén et al., 2001). Several cases have so far been observed both in the heat affected zone (HAZ) of the welds as well as in the base metals far away from any weld. Cracking in reactor pressure vessel head penetrations and in steam generator tubes made of a Ni-base Alloy 600 has been detected in several pressurized water reactors (PWR). The observed cracks initiated in Alloy 600 and propagated into Alloy 182 weld metal. In a number of PWR's the original pressure vessel heads with Alloy 600 penetrations have been substituted by Alloy 690 and the dissimilar metal welds in the replacement are made using Alloy 152. The intergranular stress corrosion cracking has also been observed in pipe safe-ends of BWR's made of Alloy 600 (Hänninen et al., 2006). Several open questions are still connected to these types of stress corrosion cracking, such as the effect of cold work (amount and temperature), the influence of constraint during welding, a possible difference in the behaviour between different types of steels and alloys, etc. Although all affecting parameters are so far not known, deformation seems to be a common parameter. Among the others, the affecting deformation mechanisms involve dynamic strain ageing (DSA), which is the objective for the present study.

1.1 Dynamic strain aging

1.1.1 General aspects

It is well known that at a sufficiently high temperature in metals and alloys aging processes occur due to interaction of solute atoms with dislocations or in other words pinning of dislocations by solute atoms and in this way increasing the necessary stress for the dislocation movement. As a consequence of aging an increase in the yield strength and hardness of the material is usually observed. The processes of aging occur slowly near room temperature and more rapidly at higher temperatures, because diffusion of the elements responsible for ageing is aided by raising the temperature. When the ageing processes occur in alloys containing solute atoms, which can rapidly and strongly segregate to dislocations and lock them during straining, the phenomenon is commonly referred as *dynamic strain ageing* (DSA). The maximum effect of DSA corresponds to such conditions, where the solute atoms can follow by diffusion the changes of the dislocation structure. Known physical manifestations of DSA are as follows: serrated plastic flow (or abrupt changes in stress observed on stress-strain curves during deformation); negative strain rate sensitivity; blue brittleness; maximum in the variation of ultimate tensile strength and strain hardening with temperature; and peak in the variation of Hall-Petch slope with temperature (Rodriguez, 1984). Strain localisation and increased strain hardening rate, which are observed during inhomogeneous plastic flow, affect the mechanical performance of the materials in terms of ductility and time to fracture at low-cycle fatigue in constant strain mode.

Serrated flow or in other words instabilities in plastic strain are caused by instantaneous increase in plastic strain. Physical processes, which can result in a sudden increase in the plastic strain, are as follows:

1 – The plastic strain rate under dislocation glide is given by $\dot{\varepsilon}_p = \rho_m \cdot b \cdot \bar{v}$, where ρ_m is the density of mobile dislocations, $\bar{v}$ - average velocity of dislocations and b is the

Burgers vector. Therefore, discontinuous plastic flow will occur whenever there is a sudden increase in dislocation density or in the velocity of dislocations or in both.

2 – In alloys undergoing order-disorder transformations, modulations or gradients in order can interact with moving dislocations and result in serrated flow (Mannan & Rodriguez, 1972; Samuel & Rodriguez, 1975, 1980).

3 – Another phenomenon that can cause serrations is twinning, which was reported for Fe-25% Be alloy (Bolling & Richman, 1965). Serrations resulting from twinning are characterised by positive temperature dependence and negative strain rate sensitivity, which is the same for discontinuous plastic flow resulting from DSA.

4 – Another possibility is a sudden increase in the specimen temperature due to adiabatic heating when the dissipation of heat is restricted (Kubin et al., 1982).

5 – Serrated flow can also be caused by stress or strain induced phase transformation.

1.1.2 Classification and morphology

The plastic flow becomes unstable in the dynamic strain aging temperature range. This is manifested by discontinuous (or serrated) plastic flow in the stress-strain curve. These irregularities were first studied in detail by Portevin and Le-Chatelier in aluminium alloys (Portevin & Le Chatelier, 1923). Now the phenomenon associated with these serrations is called the *Portevin-Le Chatelier effect* (PLC). In general, two types of instabilities are associated with strain aging: Lüders front and the Portevin-Le Chatelier (PLC) effect. The Lüders front, in a tensile specimen, is delineation between plastically deformed and undeformed material (Lomer, 1952). It appears at one end of the specimen and propagates with typically constant velocity, if the cross-head velocity of the test machine is kept constant, towards the other end (Butler, 1962). The nominal stress-strain curve appears smooth during the propagation. However, the localization is preceded by yield point behaviour; after reaching a peak, the flow stress quickly drops

to a lower value. The PLC effect, on the other hand, is seen either as a sequence of shear bands appearing sequentially with sometimes regular spacing, or as a set of propagating bands with a source at one end of specimen (Chibab et al., 1987). The resulting nominal stress-strain curve is serrated; stress and plastic strain oscillate. During the oscillations, the average stress may remain constant or increase, either steadily or in steps corresponding to the crossing of the specimen length by the bands, indicating continuous strain hardening. These serrations may be of several types. Five types of discontinuous plastic flow due to DSA denoted as A, B, C, D and E have been reported (Figure 1).

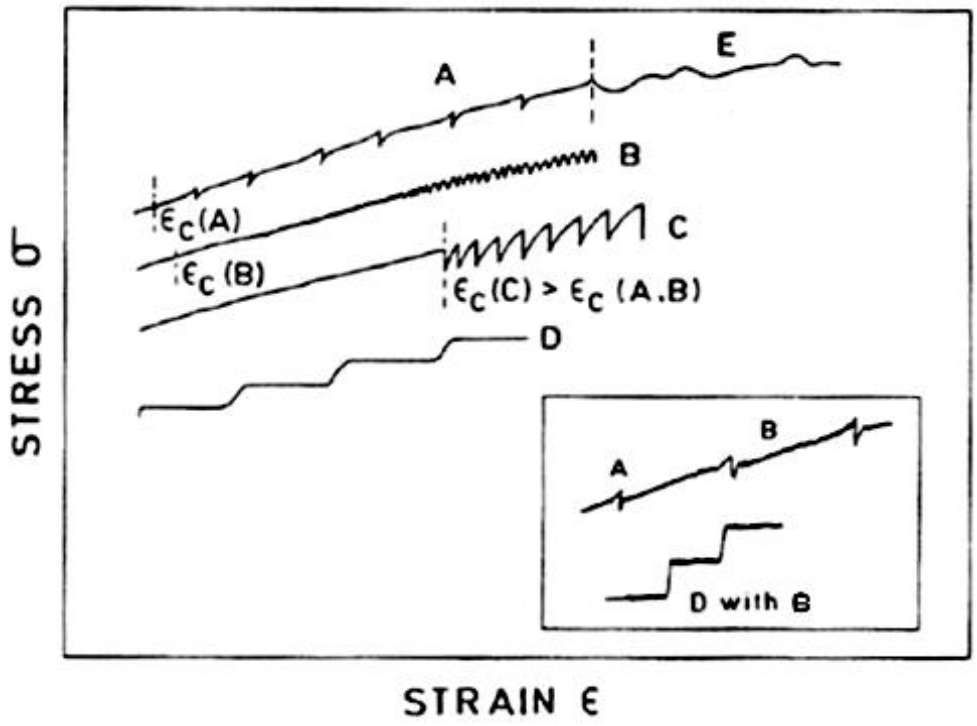

Figure 1. Stress-strain curves illustrating the various types of serrations. (Rodriguez 1984)

A-type serrations are periodic serrations, which result from the repeated nucleation of a shear band at the peak stress and then continuous propagation of the band along the gauge length in the direction of straining. These are considered as locking serrations,

characterised by an abrupt rise followed by a drop of stress below the general level of stress-strain curve. They occur in the low temperature (high strain rate) part of the DSA regime.

B-type serrations, which are oscillations about the general level of the stress-strain curve that occur in quick succession, result from the nucleation of narrow shear bands at the peak stress, which propagate discontinuously or do not propagate, and then, at the next peak, another shear band is nucleated either in an adjacent section or at some distance from the first. B-type serrations can develop from those of A-type at higher strain values or start immediately with plastic flow at higher temperatures and lower strain rates than in the case of A-type. In practice, serrations may be mixed being combinations of A- and B-type (de Almeida et al., 1998; Rodriguez, 1984).

C-type serrations are stress drops that occur below the general level of the flow curve and are therefore considered to be caused by dislocation unlocking. They occur at higher temperatures and lower strain rates than in the case of A- and B-type of serrations.

D-type serrations are plateaus in the stress-strain curve, also called “staircase type” (Hähner & Rizzi, 2003), which appear due to shear band propagation with no work hardening or strain gradient in front of the moving band. D-type serrations can also occur in a mixed mode with the B-type.

E-type serrations are similar to the A-type, but do not result in work hardening during band propagation. Plastic flow instabilities of E-type appear from the A-type at high values of strain.

A-, B-, C- and E-types of discontinuous plastic flow are observed, when a tensile test is run under CERT mode, while D-type can be observed, when the test is carried out in stress control mode (the loading either is kept constant or is increased with constant rate).

1.1.3 Models of DSA

It has been about 60 years since Cottrell and Bilby (1949) proposed that strain ageing effects are due to the segregation of interstitial solutes to form atmospheres around dislocations, which then require an increased force to break away from these atmospheres to become mobile. There is, however, no clear consensus yet as to details of the mechanism of the DSA, although the Cottrell model became the basis for much of the study of strain ageing. Three different approaches have been used in modeling of the DSA: the "solute dragging model", "arrest model" and "pair reorientation model" (also known as “Snoek locking” or “Schoeck – Seeger locking” mechanism).

In Cottrell's solute dragging model, an impurity atmosphere is formed during dislocation movement. Cottrell (1953) postulated that this mechanism can operate even at temperatures that are too low for bulk solute diffusion, as diffusion can be assisted by excess of vacancies generated during plastic deformation and the average velocity of dislocations decreases with plastic straining due to increase of dislocation density. According to Cottrell model, unstable plastic flow will initiate when:

$$\dot{\varepsilon} = \frac{4b\rho_m C_v D_0}{l}\exp(-Q_m / k_B T) \qquad (1.1-1)$$

where $\dot{\varepsilon}$ is the strain rate, C_v is the vacancy concentration, D_0 is the diffusion frequency factor, l is the effective radius of the solute atoms atmosphere, b is a Burgers vector, ρ_m is the density of mobile dislocations, Q_m is the effective activation energy for solute migration, T is temperature (K) and k_B is the Boltzmann’s constant.

Increase in vacancy concentration and in dislocation density with strain can be expressed by following equations:

$$C_v = K\varepsilon^m \quad \text{and} \quad \rho_m = N\varepsilon^\beta \qquad (1.1-2)$$

where K, m, N and β are materials constants

Then critical strain (ε_c) to initiate DSA can be expressed by substituting equations (1.1 – 2) into (1.1 – 1), which gives:

$$\varepsilon_c^{m+\beta} = \frac{l\dot{\varepsilon} \exp(Q_m / k_B T)}{4bKND_0} \qquad (1.1 - 3)$$

Although this theory is able to predict qualitatively the temperature and strain rate dependence of the onset of serrated yielding, it has been shown that the critical strain (ε_c) for the start of serrated yielding as calculated from this theory is in error by several orders of magnitude (McCormick, 1972). Moreover, the solute drag model does not predict the effect of solute concentration on ε_c or on DSA in general.

In the arrest model developed by McCormick (1972) it is considered that the motion of a dislocation on its slip plane is a discontinuous process. The dislocation meets obstacles which have to be surmounted, possibly with the help of thermal activation. A dislocation segment has to wait for a certain average time t_w until the obstacle is overcome, and after surpassing it jumps at a high velocity to the next obstacles. Diffusion of solute atoms to the dislocations may occur during the waiting time. As a consequence of DSA, the relation between stress, strain and strain rate will be affected. At constant strain rate the needed stress to keep the dislocations moving will increase due to DSA. As the waiting time is directly related to strain rate, the dependence of stress on strain rate will also be influenced by DSA. This treatment is based on the idea that the moving dislocations will be or not pinned depending on solute concentration in dislocation core which depends on the waiting time and the solute diffusion coefficient. This concept is developed to give the dependence of stress on strain rate, strain, and temperature in the presence of DSA and to formulate a criterion for the start of the Portevin-Le Chatelier effect.

The time which dislocation moves from obstacle to obstacle is assumed negligibly short in comparison to the waiting time of the dislocation in front of an obstacle. Thus, the average velocity of dislocation motion may be expressed as:

$$\bar{v} = \frac{L}{t_w} \qquad (1.1-4)$$

where L is the average distance between arresting obstacles and t_w is the waiting time. The strain rate at which the material can deform due to dislocation motion is proportional to the average velocity of mobile dislocations multiplied by dislocation density, which considering equation (1.1 – 4) gives:

$$\dot{\varepsilon} = \frac{L}{t_w}\rho \cdot b \qquad (1.1-5)$$

or for the waiting time:

$$t_w = \frac{L}{\dot{\varepsilon}}\rho \cdot b \qquad (1.1-6)$$

In this model, DSA in the solid solutions is described as diffusion of solute atoms to mobile dislocations, temporarily arrested at obstacles. The time to lock a dislocation by diffusion of solute atoms to dislocation core, for elastic solute-dislocation interactions and for short aging times, was estimated by Friedel (1964) as:

$$t_a \approx \left(\frac{C_1}{\alpha C_0}\right)^{3/2} \frac{k_B T b^2}{3DU_m} \qquad (1.1-7)$$

where t_a is aging time, C_1 is the solute concentration at the dislocation core which is required to lock it, C_0 is the solute concentration of the alloy, α is constant, D is the solute diffusion coefficient, U_m is the binding energy of solute atom to dislocation. At

the critical strain when DSA occurs it is assumed that $t_w \approx t_a$. Combination of equations (1.1 – 6) and (1.1 – 7) and taking $D = C_v D_0 \exp(-Q_m/k_BT)$ yields:

$$\dot{\varepsilon} = \left(\frac{\alpha C_0}{C_1}\right)^{3/2} \frac{3L\rho U_m C_v D_0 \exp(Q_m / k_B T)}{k_B T b} \qquad (1.1 - 8)$$

which can be expressed using equations (1.1 – 2) in terms of the critical strain as:

$$\varepsilon_c^{m+\beta} = \left(\frac{C_1}{\alpha C_0}\right)^{3/2} \frac{\dot{\varepsilon} kT\, b \exp(Q_m / k_B T)}{3LNKU_m D_0} \qquad (1.1 - 9)$$

As a consequence the solute concentration experienced locally by the dislocations depends on the arrest time and the solute diffusion coefficient. Based on the ideas suggested by McCormick (1972) and Penning (1972) the dependence of flow stress on the strain rate, the onset of serrated yielding, temperature dependence of the flow stress, effect of DSA on work hardening and strain rate sensitivity were analysed in detail by van den Beukel (1975). The theory of flow localization due to dynamic strain aging was developed further and validated with the experimental results obtained on Fe-C and Au-Cu alloys by McCormick (1988).

In the pair reorientation model, introduced by Rose and Glover (1966) and based on the Snoek (1941) theory, dislocation movement is postulated to be impeded by the interaction between the dislocations and vacancy-solute atom pairs. In this last model, long-range solute diffusion is not required. All these models predict the drops in flow stress under conditions of DSA on the basis either of dislocations breaking away from the pinning atoms or of new dislocations being formed.

In the DSA temperature and strain rate range an unusually high dislocation density is observed coupled with the immobilization of many of the dislocations by solute atoms. Large yield drops are then related to the generation of a large number of new

dislocations. The precise mechanism of this is related to the effectiveness of the locking of pre-existing dislocations, which substantially will raise the stress necessary to cause dislocation movement. If the pinning is weak, then the yield point effect can also arise as a result of unpinning and break away of dislocations of their solute atmospheres. When the pre-existing dislocations are strongly locked either by solute atoms or precipitates, the yield point effect and serrations result from a rapid generation of new dislocations.

1.1.4 Role of hydrogen in DSA

Deformation-induced vacancies ("vacancy model"), which are the diffusion vehicles for the substitutional solute atoms, can play an important role in the DSA process especially in FCC-alloys. However, strain-induced vacancies are not expected to accelerate the diffusion of interstitial atoms (Rose & Glover, 1966). Therefore, the importance of prior strain in inducing serrated flow has been explained as follows: vacancies form interstitial-vacancy pairs, which order in the stress-strain fields of dislocations and if substitutional-interstitial complexes (Mn-N, Mn-C) are involved, vacancies are necessary to increase the mobility of substitutional atoms. Recently, deformation-induced generation of vacancies and their clustering has been considered to be promoted by hydrogen and to play a primary role in hydrogen trapping and hydrogen embrittlement susceptibility in many FCC- and BCC-metals and alloys. A substantial density of vacancies can be expected in plastic strain of steels under the presence of hydrogen, which is stabilizing the vacancies. Hydrogen is lowering the formation energy of vacancies by the amount of binding energies of trapped hydrogen atoms. Formation of vacancy-solute complexes (such as H, C and N in steels) elevates the annihilation temperature of vacancies up to 200 ºC and higher (Iwamoto & Fukai, 1999; Nagumo et al. 2000). Due to the low migration energy of vacancies in Fe (53 kJ/mol) marked diffusion distances in the crack-tip regions are attainable in short time. Extra vacancies are introduced in the crack-tip plastic zone region in addition due to hydrogen in environment assisted cracking (EAC) by oxidation reactions producing vacancies at the oxide metal interface, which are injected into the base metal in the crack-tip region,

as well. The extra vacancies produced by hydrogen uptake and oxidation may be more important in causing the brittle-like EAC fracture than hydrogen itself due to their agglomeration to clusters and small voids as was already proposed by Oriani (1972). It has also been observed that if steels susceptible to hydrogen embrittlement (HE) are tested in conditions, which promote DSA, the ductility decreases remarkably by the simultaneous effects of DSA and HE (Kikuta et al., 1982). The model of synergetic effect of DSA and hydrogen entry on the embrittlement of reactor pressure vessel (RPV) steels in high temperature water was suggested by Atkinson & Yu (1997) and it is schematically illustrated in Figure 2.

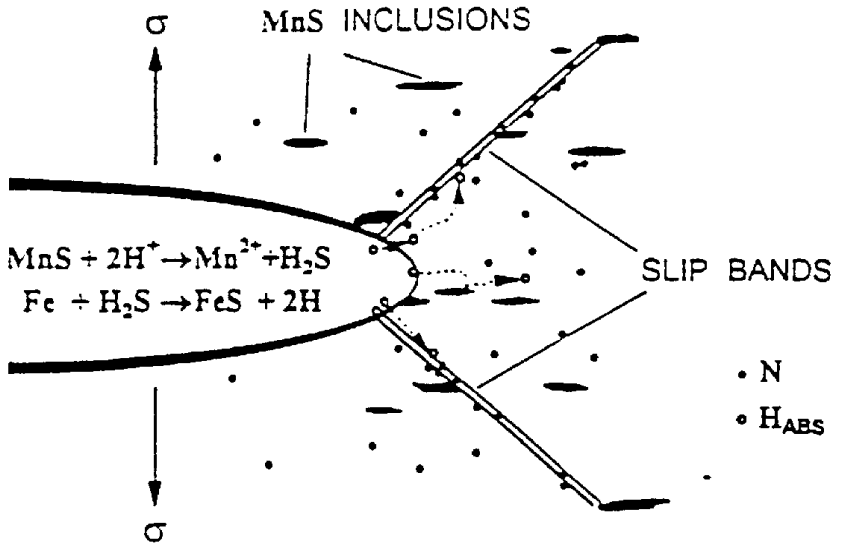

Figure 2. Schematic illustration of the synergetic effect of dynamic strain ageing and hydrogen entry on the embrittlement of reactor pressure vessel steels in high temperature water. (Atkinson & Yu 1997)

It is believed that the hydrolysis of dissolved MnS inclusions will produce H_2S and further release hydrogen atoms by the reaction of H_2S with the steel matrix. The synergism of DSA and hydrogen entry promotes the embrittling effect on steels. The supporting evidence is that the crack path of A533B or A508 steels in high temperature water above 175 ^{o}C was consistently transgranular quasi-cleavage (Atkinson & Forrest, 1985). Zig-zag cracking accompanied by subcracks and macro-crack branching was

observed in the same temperature range (Katada & Nagata, 1985). Plastic deformation exposes the crack tip to dissolve MnS inclusions and, simultaneously, results in the plastic zone ahead of the crack tip to form the slip bands along the maximum shear directions. When DSA occurs, interstitial atoms, e.g. N, reduce the mobility of dislocations at the slip bands. The hydrogen atoms that diffuse to the slip bands also embrittle the slip bands, to cause cracking. The model is consistent with the fractographic observations described above. Based on this model, a zig-zag quasi-cleavage crack path is a consequence of the repeated process of crack advancement along either of two slip bands, whichever is more favoured by stressing or embrittling condition. If both slip bands suffer almost equal embrittlement and are subjected to almost equal stress, crack branching or subcracking may take place. In unnotched specimens or plain surface condition, similar mechanisms apply, and in this case surface defects or pitting near non-metallic inclusions usually act like stress raisers (Atkinson & Yu, 1997).

1.1.5 DSA in different metals and alloys

DSA manifested by PLC effect has been observed in a variety of FCC and BCC, substitutional and interstitial alloys in particular ranges of temperatures and strain rates, as well as in non-metals such as silicon (Mahajan et al., 1979). Also the PLC effect has been observed in ordered intermetallics (Brzeski et al., 1993) suggesting a disordering near dislocations. To the present day DSA has been reported in most of the engineering materials such as low carbon steels, low-alloy steels, stainless steels, Al-, Ni-, Ti- and Zr-based alloys. Cuddy and Leslie (1972) demonstrated that the PLC effect occurs in Fe-3% Ni and Fe-1.5% Si alloys within a certain region of temperature and strain rate. The temperature of DSA occurrence is material dependent, e.g. for low-alloy steel serrations are observed at 140-340 °C (Kim & Kang, 1995), in austenitic stainless steels they occur in the range 300 to 650 °C (Kim et al., 1998; Hong & Lee, 2005), while in Ni-base alloys serrated plastic flow was observed at the temperatures of 200 – 600 ^{o}C (Mulford & Kocks, 1979).

At different temperatures various solute atoms and a number of mechanisms can participate in the solute atom – mobile dislocation interactions. In general, in BCC metals interstitial solute atoms cause DSA, while in FCC metals it may also be caused by substitutional solute atoms. Nitrogen and carbon and their pairs with vacancies are important at lower temperatures up to 500 ^{o}C, while DSA manifests itself as serrated plastic flow of type A in austenitic stainless steels and Ni-base alloys. At temperatures about 600 ^{o}C, where the serrations of type B and C are observed, the DSA is attributed to interaction of substitutional solute atoms (Cr or Mo) with mobile dislocations (Kim et al., 1998; Hong & Lee, 2004; 2005; Mulford & Kocks, 1979; Chen & Chaturvedi, 1997).

DSA in carbon and low-alloy steels

Effects of DSA observed in mild steels in CERT testing were summarised by Baird (1973) giving typical DSA manifestations on mechanical properties. An increased rate of strain hardening was observed, resulting in two peaks of UTS vs temperature. The minima in the elongation to fracture vs temperature and uniform elongation vs temperature are usually observed at temperatures somewhat below that of the peak in UTS (200 – 300 ^{o}C). The increased strain hardening rate and plateau in YS are usually also observed. Serrated flow is reported to promote pronounced oscillations of stress on stress-strain curve with the temperature increase. As the peak in strain hardening rate is passed, serrated flow disappears. The occurrence of serrated flow is associated with negative strain rate sensitivity. The temperature for the onset of serrated flow is a function of strain rate and interstitial solute concentration. For example in 0.03 % C steel, quenched from 250 ^{o}C, serrated flow was reported in the temperature range of 50 – 250 ^{o}C at strain rates of 10^{-4} – 10^{-2} s^{-1} (Keh et al., 1968). At higher strain rates, such as those obtained by impact deformation, loss of ductility or blue brittleness attributed to DSA was reported even at 400 – 670 ^{o}C for annealed 4340 steel (Clough et al., 1968). The dependency of the temperature of serrated flow set-on from interstitial concentration for mild steel was studied by Keh et al. (1968). According to the results the temperature of the appearance of the first serrations was the higher the lower the

interstitial concentration was. The activation enthalpy of serration flow set-on in 0.035% C mild steel was 83.7 kJ/mol. The temperature for the disappearance of serrations is a function of strain rate, with higher activation energy than for serration appearance, and weakly dependent on solute concentration (Keh et al., 1968). Strain aging in mild steel is largely due to nitrogen with a smaller contribution from carbon (Baird, 1973). In order to explain unstable dislocation movement, Roberts and Owen (1970) have deduced that jerky flow in ferrite is probably due to Snoek ordering of interstitial atoms around mobile dislocations, but in ferrite dislocations can not be pinned sufficiently due to Snoek ordering to increase the strain hardening rate (Baird, 1973). Thus, jerky flow is probably due to Snoek ordering but the simultaneous rise in strain hardening arises from the formation of Cottrell atmospheres around immobile dislocations, as proposed by Bergström and Roberts (1971).

In low-alloy steels (LAS), serrated flow associated with DSA was observed during plastic straining at sufficiently slow strain rates ($<10^{-2}$ s^{-1}) in the temperature range from 100 to 350 °C (Kang & Kim, 1992; Kim & Kang, 1995; Atkinson & Yu, 1996; Seifert & Ritter, 2002). The temperature range of the DSA observations varies depending on strain rate and microstructural condition of the steel (Kim & Kang, 1995). The reported values of activation energy for the DSA set-on are in the range of 75 – 85 kJ/mol being comparable to the common values for N and C diffusion in α-iron, 65 – 85 kJ/mol (Keh et al., 1968). It has been shown that the value of activation energy for the set-on of serrated flow, in general, is not sensitive to the microstructure or composition of the steel and only Mn alloying increases the activation energy for the serrated flow appearance (Li & Leslie, 1978). It was suggested that Mn influences the diffusion process of N and C by forming Mn-N and Mn-C pairs increasing consequently the activation energy for the diffusion process. In ferrite C and N are producing a nearly identical lattice misfit strain, which they can reduce by moving to the dislocation core regions, resulting in an overall reduction in the total strain energy. In ferrite N and C have similar diffusion coefficients and consequently these two elements are expected to produce nearly similar DSA effects in LAS. Therefore, in general, the effects produced by C and N can be considered as additive. For example, with a typical dislocation

density of $10^8/cm^2$ in Fe the C concentration of 10^{-6} wt. % is sufficient to provide one interstitial C atom per atomic plane along all the dislocation lines present. Thus, very small C and N contents are sufficient to form condensed atmospheres on dislocations in ferrite and cause yield point phenomena. N solubility in steel is higher at all temperatures than that of C. It is generally assumed that N, rather than C, is mainly responsible for DSA in LAS. However, at higher temperatures in the DSA range the increasing solubility of carbon may cause DSA even in the absence of N (Baird, 1973; Seifert & Ritter, 2002). Therefore, in LAS, all effects of static and dynamic strain aging are explained in terms of either segregation of interstitial solute atoms (C and N) to dislocations to form condensed Cottrell atmospheres or precipitates, or Snoek (stress induced) ordering of solute atoms in the dislocation core structure (Seifert & Ritter, 2002). Considering similar mechanisms of interstitial atom-dislocation interaction for BCC alloys the value of activation energy for the disappearance of serrations should correspond to that of the sum of activation energy for diffusion and binding energy of an interstitial atom to the dislocation core (Baird, 1973). However, the observations for LAS show often too high activation energy values for this explanation to be always true. The reported differences in the activation energy for the disappearance of DSA suggest that it is also a function of steel composition (Keh et al., 1968).

Manifestations of DSA in LAS are similar to those in other BCC alloys, such as: peak in UTS, increased strain hardening rate and negative strain-rate sensitivity are observed in the DSA temperature range. DSA results in increased hardness and in minimum of ductility. It was also observed that DSA results in an increase in the ductile-to-brittle transition temperature following plastic deformation in the DSA temperature range as well as in the lowering of the ductile fracture resistance (decrease of tearing modulus) at temperatures within the DSA temperature range (Kim & Kang, 1995). A reduction of low-cycle fatigue resistance of LAS in air and water environment is observed as the loading strain rate is decreased. Microscopically, DSA results in an inhomogeneous localization of deformation, and an increase of dislocation density (Mohan & Marschall, 1998; Kang & Kim, 1992; James & Porr, 1999).

The observed EAC behaviour of LAS in high-temperature water can be best rationalized by a combination of three fundamental cracking mechanisms: film rupture – anodic dissolution; hydrogen assisted EAC and DSA. At lower temperatures (< 100 °C) and/or high strength levels (R_p > 800 MPa) hydrogen effects are more pronounced. At high temperatures (150 °C) and/or lower yield strength levels (R_p < 800 MPa) anodic dissolution seems to dominate. Under certain combinations of temperature and strain rate DSA may give an additional contribution to the crack growth in LAS, which contain interstitial N and C (Seifert & Ritter, 2002), as the EAC data strongly suggest that the susceptibility of LAS to EAC coincides with DSA behaviour in terms of temperature and strain rate (Atkinson & Yu, 1997).

DSA in weld and HAZ material of carbon and low-alloy steels

The concentration of free interstitial C and N strongly depend on the steel production or welding processes, the thermal history or heat-treatment and on the chemical composition of the steel. Alloying elements, which have a strong affinity to N or C, such as Al, Cr and Mo, and form nitrides or carbides may result in a reduction of the concentration of free C and N in the solid solution. During the welding process uptake of O and N can occur. Thus, weld metals often have a low Al but high O content. During fast cooling after welding, incomplete precipitation of carbides and nitrides occurs resulting in an increased or even supersaturated concentration of free C and N in steels in the as-welded condition. Therefore, welds may be more susceptible to EAC in the ranges of temperature and strain rate, where DSA is observed, than generally thought so far. In heat-affected zones (HAZ) of the welds markedly higher density of dislocations to complete the deformation can be observed due to development of shrinking strains during the thermal cycle of welding and in later loading in the DSA temperature range, e.g., inside of the crack tip plastic zone.

The content of interstitial C and N atoms in solid solution of the weld metals can strongly vary depending on the heat treatment and on chemical composition (C_{total}, N_{total}, Cr, Mo, V, …). Alloying elements, which have a strong tendency to form carbides

as Cr or Mo may also affect the residual interstitial carbon content. In the heat-affected zone near to the fusion line, with high peak temperatures slightly below the melting point, partial dissolution of carbides followed by incomplete re-precipitation during subsequent cooling occurs, which can result in a supersaturated concentration of interstitial atoms in the solid solution. During the following post-weld heat treatment (stress relieving) precipitation of carbides and nitrides occurs. The concentration of interstitial carbon and nitrogen is strongly dependent on the stability of the carbides and nitrides (chemical composition) and on the parameters (time, temperature, heating and cooling rate) of the heat treatments applied. The most severe DSA effects are expected for materials in the as-welded condition without post-weld heat treatment (e.g., repair welding). Thus, the post-weld heat treatment temperature is critical (Seifert & Ritter, 2002). Differences in free N and C content of otherwise identical or similar steels may be an important further reason for the scatter of EAC crack growth rate data, and especially for the observed different trends in the temperature dependence of EAC. Due to the of possible DSA effects, a higher EAC susceptibility of weld metals and weld HAZ materials compared to base material cannot be excluded in the DSA temperature/strain-rate range (Hänninen et al., 2001; Seifert & Ritter, 2002).

DSA in Ni and Ni-base alloys

In Ni-C alloy, dynamic strain aging was for the first time reported by Nakada and Keh (1970). Serrated flow was observed in the temperature range of -50 – +300 ^{o}C. The appearance of serrations was dependent on temperature, strain rate and solute concentration, while the temperature and strain rate at which serrations disappear were found to be independent on carbon concentration. The apparent activation energies for set-on and disappearance of serrated flow were determined as 63 ± 8 kJ/mol and 109 ± 17 kJ/mol, respectively. As the determined activation energy for the appearance of serrations was only one half of the activation energy for the bulk diffusion of C in Ni, it was proposed that this activation energy is related to pipe diffusion of C atoms along dislocations cores, which is the rate-controlling mechanism of DSA in Ni-C alloys. It was also concluded that in contrast to the FCC substitutional alloys, the type and level

of serrations were not dependent on the concentration of quenched-in vacancies. Similar conclusion was drawn by Kocks et al. (1985), who studied strain aging and strain hardening in Ni-C alloys. It has been concluded that vacancies are rarely, if ever responsible for the strain dependence of aging phenomena, which is caused instead due to a strong synergetic solute hardening and strain hardening (Kocks et al., 1985). The activation energy for the termination of serrations was explained as the sum of the activation energies for the diffusion of C in Ni plus the binding energy of the C atom to a dislocation in Ni, which was estimated as 46 kJ/mol. Serrated flow was also studied in Ni-H, Ni-H-C and Ni-C alloys by Kimura and Birnbaum (1990) in a wide range of temperatures (-196 – 300 ^{o}C) and strain rates of 4.4×10^{-3} – 2.8×10^{-7} s^{-1}. The temperature and strain rate ranges of serrated flow observations in Ni-C alloy are in good agreement with the results reported by Nakada and Keh (1970). The reported activation energies for the commencement and termination of serrated flow related to C diffusion in Ni were 60 kJ/mol and 110 kJ/mol, respectively, which is also in agreement with the previously reported results. Thus, the same mechanism of DSA due to C solutes was considered. Kimura and Birnbaum (1990) have also concluded that the serrated flow caused by C is not affected by the presence of H in solution, while the presence of C resulted in an increase of temperature at which serrated flow due to H solutes commences. In Ni-base Alloy 600 serrated flow related to DSA was reported in the range of temperature from 150 ^{o}C to 600 ^{o}C depending on the strain rate (Mulford & Kocks, 1979; Hayes & Hayes, 1982; Hong et al., 1996). Hayes and Hayes (1982) have reported values of the activation energy for the appearance of serrations in the range of 54 – 58 kJ/mol, which was consistent with previously obtained results for Ni-C alloys (Nakada & Keh, 1970), thus the same mechanism to explain DSA was considered. Hong et al. (1996) have reported five different types of serrations: A1, A2 (can be also identified as A+B), B, C and E which were observed depending on temperature, strain and strain rate. The values of activation energies for the onset of serrated flow of types A1, A2 and B were calculated separately. The reported values were 93 – 127 kJ/mol for type A1 (observed in the temperature range of 150 – 245 ^{o}C); 72 – 87 kJ/mol for type A2 (A+B) (temperature range of 245 – 400 ^{o}C); and 144 – 163 kJ/mol for B-type (245 – 500 ^{o}C). From the values of activation energies the rate controlling mechanisms for

DSA were suggested as the migration of substitutional atoms (Ti) assisted by vacancies for serrations of type A1, carbon diffusion through dislocation core for the mixed mode (A2 or A+B) and carbon diffusion through lattice for B-type serrations.

Oxidation-induced intergranular cracking and Portevin–Le Chatelier effect have been extensively studied by Fournier et al. (2001) in Ni-base superalloy 718. Serrated flow of C-type, characterised by a partly plastic reloading sequence and an audible acoustic emission, was observed at temperatures between 400 and 470°C. It was shown that in this temperature domain fracture occurs by extensive shearing on a macroscopic plane inclined 45° to the tensile axis. The abrupt transition from type C plastic instabilities to continuous plastic flow in the temperature regime between 470 and 500°C coincides with a transition from pure mechanical failure to EAC. A specific CERT test making use of this abrupt transition in this narrow temperature range allowed investigation of the interactions between oxidation and plasticity responsible for the oxidation-induced intergranular cracking process. It was concluded that in Ni-base superalloy 718 the plastic deformation mode has a strong influence on the environmental effect, which is controlled by the local strain rate rather than by the local stress at the crack tip.

DSA in austenitic stainless steels

Experimental aspects of the PLC effect and DSA have been extensively studied in the following grades of austenitic stainless steels by many authors: 303-type (de Almeida et al., 1994), 304-type (de Almeida et al., 1994, 1998; Venugopal et al., 1997; Stewart & Jonas, 2004; Byun et al., 2004), 316-type (Mannan et al., 1983; Kim et al. 1998a, b, 2003; Alain et al., 1997; Gerland et al., 1997; Hong and Lee, 2004a, b, 2005; Samuel et al. 1988; Samuel et al., 2002; Byun et al., 2004; Srinivasan et al., 1997, 2004) and 310-type (Shi & Northwood, 1995).

In austenitic stainless steels DSA was reported in a wide range of temperatures depending on the strain rate. The DSA was observed from about 200 ^{o}C up to 800 ^{o}C and in 303 and 304 stainless steels it separates into two sub-ranges at strain rates higher

than 10^{-5} s^{-1}, where A-, B- and mixed (A+B)-type of serrated flow have been reported (de Almeida et al., 1994, 1998), while for 316-type austenitic stainless steel all types of serrated flow and their mixed modes were reported (Mannan et al., 1983; Samuel et al. 1988; Hong and Lee, 2004a; 2004b; 2005). Values of activation energy for the set-on and ending of serrated flow vary depending on chemical composition, test conditions and on the approach, by which the activation energy was calculated. Strain rates and temperature ranges where serrated flow was reported in austenitic steels along with thecorresponding activation energies are summarised in Table 1. In austenitic stainless steels of type 303, 304, 316 and 330, the values of activation energy for the appearance of serrated flow of type A in the temperature range of about 260 – 360 ^{o}C were reported to be in the range of 134 – 142 kJ/mol (de Almeida et al., 1994, 1998; Samuel et al., 1988; Jenkins & Smith, 1969). Also much lower values of 75 – 98 kJ/mol were obtained for 316L steel and 109.5 kJ/mol for 316LN steel (Hong & Lee, 2005a; Kim et al., 1998). Venkadesan et al. (1992) have reported activation energy of ~115 kJ/mol for the appearance of serrations in 15Cr-15Ni-Ti modified austenitic stainless steel and values in the range of 83 – 111 kJ/mol were reported for Fe-Ni-C alloys (Rose & Glover, 1966; Jenkins & Smith, 1969). In all the studied alloys, these values of activation energies were by most of the authors (Rose & Glover, 1966; Jenkins & Smith, 1969; de Almeida et al., 1994, 1998; Kim et al., 1998) related to vacancy migration, which controls the carbon-vacancy pair reorientation mechanism of aging, originally suggested to explain DSA by Rose and Glover (1966). Samuel et al. (1988) have related obtained activation energy (133 – 138 kJ/mol) to self diffusion energy of carbon or nitrogen. De Almeida et al. (1994) have argued that even these values of activation energy are close to those for self diffusion of C or N in pure Ni or γ-Fe, but in multicomponent alloys where Cr is present as an alloying element the activation energy of carbon self diffusion should be higher. The activation energy of 195 – 205 kJ/mol was obtained for the set-on of serrated flow of type A in the temperature range of 465 – 700 ^{o}C (2^{nd} range) and it was related to C or N self diffusion only. This conclusion was made by comparing the obtained values to the activation energy of 187 – 205 kJ/mol reported by Agarwala et al. (1970) and Ismail et al. (1981) for the diffusion of carbon in 304 stainless steel and

Table 1. Activation energy data for the serrated flow in austenitic steels from published literature.

Type of steel	Reported type of serrations	DSA temperature range, ^{o}C	Strain rate, s^{-1}	Corresponding activation energies of DSA, kJ/mol		Reference
				Initiation	Termination	
303	A, A+B	256 – 360 465 - 675	3.5×10^{-4}	142 (1^{st} range) 205 (2^{nd} range)	314	de Almeida et al. (1994)
304	A A B	265 – 375 475 – 700	3.5×10^{-4}	135 (1^{st} range) 195 (2^{nd} range) 240	418	de Almeida et al. (1994, 1998)
316 NG	A, B, C	450 – 600	3×10^{-4}	255	---	Mannan et al. (1983)
316	A, B, C	250 – 650	$10^{-4} – 10^{-3}$	133 – 138	277 – 278	Samuel et al. (1988)
316L	A, B	~ 300 – 600	2×10^{-4}	98	272	Kim et al. (1998)
316LN	A, B	~ 350 – 650	2×10^{-4}	109.5	320	Kim et al. (1998)
316L (CW)	D A+B A+B+C	250 – 550 450 – 650 550 – 700	$10^{-4} – 10^{-2}$	75 182 205	227	Hong and Lee (2005a)
310	---	300 - 600	5×10^{-5} – 5×10^{-1}	81.3 – 93.8*	307.8 – 358.7*	Shi & Northwood (1995)
330	A, B, C	200 – 675	3×10^{-5} – 3×10^{-3}	134 ± 17	418 ± 42	Jenkins & Smith (1969)
Fe-35Ni-C	---	100 - 300	3×10^{-5} – 3×10^{-3}	111 ± 17	259	Jenkins & Smith (1969)
Fe-35Ni-15Cr	---	450 – 675	3×10^{-5} – 3×10^{-3}	142 ± 17	389	Jenkins & Smith (1969)
Fe-32Ni-C	A+B	100 – 250	$10^{-5} – 10^{-3}$	83	---	Rose & Glover (1966)
15Cr-15Ni-Ti mod.	A A C	300 – 350 450 – 600 500 – 650	6.3×10^{-5} – 1.26×10^{-2}	115 ± 9 140 ± 7 178 ± 7	251	Venkadesan et al. (1992)

* - the values correspond to activation energy for the plastic flow process, which was calculated from the yield stress results

work of Askill (1965), who suggested that activation energies for carbon and nitrogen diffusion in austenite should be equivalent.

De Almeida et al. (1994, 1998) related the activation energy of 240 kJ/mol for the set-on of B-type serrations in 304 steel in the temperature range of 475 – 700 ^{o}C to Cr diffusion by comparing it to the value reported by Lai (1983) for Cr diffusion in austenitic stainless steels (244 kJ/mol) at temperatures of 575 – 685^{o}C. Lai (1983) also showed that the process of carbide precipitation in stainless steels is controlled by Cr diffusion and noted that at the lower temperatures the nucleation rate of carbides is high but growth is slow, while at higher temperatures both processes are rapid. Thus, transition from A-type to B-type serrations with increasing temperature and decreasing strain rate was explained by an increase in the mobility of interstitials or defect pairs allowing them to move with the same rate as dislocations and by the precipitation of fine carbides, which results in a partial depletion in the free carbon concentration. It was also concluded that values of activation energy of 314 – 418 kJ/mol obtained for the termination of serrated flow are not related to the mechanism leading to the end of DSA, which was explained by the depletion of interstitials due to precipitation of carbides and increase in self-diffusion, allowing the pinned dislocations to overcome obstacles by climb (de Almeida, 1994, 1998).

Hong & Lee (2005a) have also related the activation energy for the appearance of serrated flow (75 kJ/mol) to diffusion of N or C, with reference to work of Samuel et al. (1988). The difference in activation energies was explained by Hong and Lee (2005a) who reported rather close values of activation energy of 182 kJ/mol and 205 kJ/mol for cold-worked 316L austenitic stainless steel to those reported by de Almeida (1994, 1998), but attributed these activation energies to pipe diffusion of Cr atoms.

In the work of Rose and Glover (1966) on strain aging in Fe-Ni-C alloys the activation energy for the DSA set-on was calculated as 83 kJ/mol. Such low activation energy was attributed to the diffusion of vacancies, which was estimated based on the assumption that activation energy for vacancy diffusion is approximately one third of activation

energy for self diffusion (280 kJ/mol), or could be compared to the activation energy of vacancy diffusion in copper (65 kJ/mol) by assuming that the ratio of activation energy to melting temperature is constant for the same point defect in the same crystal structure. Both estimations provide values of activation energy for vacancy diffusion in the range of 80 – 90 kJ/mol, which is close to the obtained value. It was also reported that strain aging process occurs in austenite at room temperature and that it is more rapid at temperatures above 100 ^{o}C. Thus, strain aging mechanism was explained by formation and reorientation of carbon-vacancy pairs in the stress fields around dislocations, which occurs by movement of vacancies. This mechanism of strain aging was compared with Snoek-like relaxation in FCC alloys (Rosin & Finkelstein, 1953; Verner, 1965), which is attributed to relaxation processes caused by the reorientation of point defect pairs (carbon – carbon; carbon – substitutional element or vacancy). This type of aging was also analysed in detail for α-iron by Schoeck and Seeger (1958) and nowadays it is referred as "Snoek locking" or "Schoeck – Seeger locking" mechanism.

In 310 austenitic stainless steel negative SRS was reported for temperature range 300 – 600 ^{o}C at strain rates of 5×10^{-1} – 5×10^{-5} s^{-1} (Shi & Northwood, 1995). The plateau in YS dependency on temperature and increase of UTS with temperature was reported at the strain rate of 5×10^{-5} s^{-1} at temperatures of 300 – 500 ^{o}C. The activation energies for dislocation segment to overcome obstacles were calculated from the yield stress results obtained at strain rate of 5×10^{-5} s^{-1} and temperature range of 60 – 650 ^{o}C. The results have shown two distinctive regions: low activation energy region at temperatures below 350 ^{o}C with values of activation energy of 81.3 – 93.8 kJ/mol; and high activation energy region reported for temperatures above 450 ^{o}C with values of activation energy of 307.8 – 358.7 kJ/mol.

The DSA in nitrogen-alloyed 316L austenitic stainless steel was studied by Kim et al. (1998, 2003). The mechanical properties of steels with different nitrogen contents of 0.01, 0.04, 0.10 and 0.15 wt. % were compared by means of tensile tests at temperatures from room temperature up to 750 ^{o}C and strain rates of 1×10^{-2} – 2×10^{-4} s^{-1} (Kim et al., 1998). It was shown that nitrogen alloying increases yield and tensile strength of the

steel without reduction in ductility. It has been found that nitrogen alloying shifts temperature range of serrated flow observation to higher temperatures. The reported temperature ranges of serrated flow at strain rate of 2×10^{-3} s^{-1} were 400 – 600 ^{o}C for steel with 0.04 % of N and 500-700 ^{o}C in the case of steel with 0.1% of N. Only serrations of A- and B-type were observed. The reported activation energy for serrated flow appearance was 97.8 and 109.5 kJ/mol for 316L steel with 0.1 and 0.10 wt. % of N, respectively, which was attributed to the diffusion of vacancies. The activation energy for the end of serrations was 271 and 320.2 kJ/mol for 0.1 and 0.10 wt. % of N, respectively. The increase in LCF life of the steel and decrease in crack propagation rate with nitrogen alloying was also reported in (Kim et al., 2003). The dislocation structure of the steel after LCF test at total strain range of 1 % was different depending on nitrogen content and regardless of test temperature. At 0.04 wt.% of N the cellular dislocation structure was observed, while at 0.1 wt. % of N planar dislocation structure was reported. The larger increase of LCF life at 600 ^{o}C than that observed at RT with addition of nitrogen was attributed to the retardation of DSA by addition of nitrogen.

DSA was investigated in 17% cold worked 316L stainless steel by Hong and Lee (2004a, 2004b, 2005) by means of tensile and LCF tests. Effect of DSA was reported as plateau in the yield strength and UTS dependencies on temperature. A minimum in ductility and negative strain rate sensitivity were reported in the temperature range of 250 – 600 ^{o}C for all applied strain rates, while type of serrations and temperature ranges of their observation were dependent on strain rate. Serrations were attributed to D-type at lower temperatures and to a mix of A+B+C-type and A+B+C+E-type at higher temperatures. The corresponding activation energy for each type of serration were 75.3 kJ/mol for type D-type, 182.2 kJ/mol for type A+B+E serrations, and 205.3 kJ/mol for type A+B+C+E serrations. The D-type serrations observed at temperatures of 250 – 550 ^{o}C were suggested to occur due to pinning of dislocations by interstitial atoms such as C or N, which diffuse to unpinned dislocations by means of the pipe diffusion through a forest of dislocations. The pipe diffusion of substitutional Cr along the dislocation core was suggested as the rate controlling mechanism for type A+B+E and type A+B+C+E serrations, which appeared at temperatures of 450 – 700 ^{o}C.

Cyclic stress response at all test conditions was characterized by an initial hardening during the few cycles, followed by gradual softening until failure. Temperature and strain rate dependence of cyclic softening appears to come from a change of the cyclic plastic deformation mechanism and the DSA effect. The regimes of DSA between tensile and LCF loading conditions in terms of the negative strain rate sensitivity were consistent with each other. At the elevated temperature, a drastic reduction in fatigue resistance was observed, and this was attributed to the effects of oxidation, creep, and dynamic strain aging and interactions among these factors. TEM studies of dislocation microstructure showed that LCF test conducted at temperatures of 400 ^{o}C, where negative SRS was observed, resulted in planar dislocation structure, while after the test at room temperature and at the temperature of 600 ^{o}C observed dislocation structure was cellular (Hong & Lee, 2005a).

Instantaneous work hardening rate $d\sigma / d\varepsilon$ and $\sigma \times d\sigma / d\varepsilon$ vs σ were analyzed for nitrogen-alloyed 316LN austenitic stainless steel by Samuel et al. (2002) in the range of temperatures from 27 ^{o}C to 850 ^{o}C and strain rates of 3×10^{-5} - 3×10^{-3} s^{-1}. It has been shown that dependencies of $\sigma \times d\sigma / d\varepsilon$ from σ obtained for temperatures below 800 ^{o}C can be divided into three stages: an initial transient stage, where $\sigma \times d\sigma / d\varepsilon$ decreases rapidly, second stage where $\sigma \times d\sigma / d\varepsilon$ increases gradually with stress to a maximum and third stage where $\sigma \times d\sigma / d\varepsilon$ decreases. The second stage was not evident from the plots of $d\sigma / d\varepsilon$ vs σ, but was clearly recognised in $\sigma \times d\sigma / d\varepsilon$ vs σ dependencies. The second stage was not observed at temperatures over 800 ^{o}C. In the transient stage, with increasing stress both dislocation velocity and mobile dislocation density increase leading to rapid increase in plastic strain rate immediately after elastic limit. This stage in austenitic stainless steels has been attributed to the stabilisation of the plastic strain rate associated with the dislocation source density. The mechanism of the second stage was explained as activation of cross-slip and multiple slip over long-range distances, which promotes the formation of heterogeneous dislocation structures composed of tangles, walls and cells in AISI 316L stainless steel, which increases with plastic strain (Feugas, 1999). The size of these structures in terms of thickness and spacing decreases rapidly in the second stage and remains constant in the third one. During the straining at

the second stage, tangles and walls disappear progressively and cells represent main part of heterogeneous structure in stage three. Proposed mechanism of rapid increase in dislocation density in stage two with plastic strain was also reported by Feugas (1999) for AISI 316L stainless steel, which explains the observed hardening in the second stage. It has been found that this stage has the athermal nature as $\sigma \times d\sigma / d\varepsilon$ vs σ dependencies in the range of temperatures from 250 ^{o}C to 600 ^{o}C and strain rate of 3×10^{-4} s^{-1} have shown nearly the same values. The recovery dominant third stage is manifested as a decrease in $d\sigma / d\varepsilon$ and $\sigma \times d\sigma / d\varepsilon$ with respect to σ with increasing temperature. It was suggested that controlling recovery processes in this stage are extensive cross-slip of dislocations at low temperatures and climb of dislocations at high temperatures. The increased rate of dynamic recovery is also exhibited by a decrease in stress for the onset of the third stage with increasing temperature and at temperatures relevant for DSA it remained almost unaltered. This suggests that in this temperature range, the onset of the third stage is also athermal. The observed variation in strain hardening in the DSA temperature regime is a reflection of the evolution of dislocation substructure due to reduced recovery.

DSA causes an increased rate of dislocation multiplication and delay in recovery of dislocation structure, and promotes an increased propensity towards uniform distribution of dislocations rather than cellular structures in many metals and alloys (Edington & Smallman, 1964; Dingley & McLean, 1967; Michel et al., 1973; Morris, 1974; Kashyap et al., 1988; Kashyap & Tangri, 1997). Kashyap et al. (1988, 1997) showed uniform dislocation distribution in the early stage of deformation and cellullar structure at high strains having dense and thick cell walls composed of dislocation tangles in type 316L austenitic stainless steel in the DSA temperature regime. Morris (1974) pointed out that the tendency to produce a non-cellular array of dislocations increases with an increase in the intensity of dynamic strain ageing. These investigations indicate reduced dynamic recovery in the DSA regime arising from the diffusion of solutes, which affects the rate of dynamic recovery by pinning of dislocations and thereby preventing screw dislocations to cross-slip due to their reduced mobility.

As it is seen from above, interstitial atoms such as carbon and nitrogen play an important role in the mechanical properties of low-alloy steel, austenitic stainless steels and Ni-base alloys. Strength, creep resistance and fatigue life of these alloys under the environmental conditions of nuclear reactors depend on the amount, state and diffusion mobility of interstitial atoms dissolved in the solid solution of the alloys. It has been shown, that due to the interaction of carbon and nitrogen with mobile dislocations, a minor content of interstitial atoms in the solid solution results in dynamic strain aging of the steels and Ni-base alloys at temperatures above 200 ^{o}C. As it is clear that strain aging in metals and alloys is associated with the time dependent segregation of mobile solutes to temporarily arrested dislocations, which partially impedes dislocation motion, the knowledge about parameters of solute diffusion is considered to be an essential part of the understanding of the DSA phenomenon. One of the methods to obtain this knowledge is mechanical spectroscopy, which is also known as internal friction measurement.

1.2 Mechanical spectroscopy

1.2.1 Anelastic behaviour of solids

In a solid material exposed to a time-dependent load within the elastic deformation range the phenomenon of internal friction is most generally defined as the dissipation of mechanical energy inside the material due to deviations from Hooke's law and is observed as stress – strain hysteresis in the case of cyclic loading (Nowick & Berry, 1972). The corresponding energy loss ΔW per cycle divided by the maximum stored elastic energy W during the cycle, defines the *specific damping capacity* $\psi = \Delta W/W$, or the *loss factor* $\Delta W/2\pi W$, which is the general measure of internal friction. The reciprocal loss factor is called the *quality factor* $Q = 2\pi W/\Delta W$, therefore the internal friction or damping is commonly denoted as Q^{-1} and can be expressed as:

$$Q^{-1} = \Delta W / 2\pi W = \psi / 2\pi \qquad (1.2-1)$$

The dependency between stress and strain for an ideal elastic material is determined by Hooke's law: $\sigma = M\varepsilon$ or $\varepsilon = J\sigma$, where σ is stress, ε – strain, M – modulus of elasticity and J – modulus of compliance, which is reciprocal to M, $J = 1/M$. In the case of ideal elastic behaviour it is assumed that the equilibrium between stress and strain is achieved instantaneously, as both are not dependent on time. The behaviour of the solid is called anelastic when a time dependent component is considered in addition to instantaneous elastic response in the stress-strain relation. According to Nowick and Berry (1972), the *anelasticity* is defined by the following three postulates:

1. For every stress there is a unique equilibrium value of strain, and vice versa.
2. The equilibrium response is achieved only after the passage of sufficient time, which can vary from less than microsecond to extremely long periods of time.
3. The stress–strain relationship is linear.

Completely recoverable three-parameter models shown in Fig. 3a are used to describe the behaviour of standard anelastic solid (or Zener solid), which can be observed as a saturating "creep" strain $\varepsilon(t)$ after loading, with unrelaxed and relaxed values of strain ε_U and ε_R and as a decaying "elastic after-effect" unloading (Fig. 3b). Anelastic relaxation can also be observed as stress relaxation in case of a constant applied strain. The time dependent self-adjustment of a solid material toward a new thermodynamic equilibrium in response to a change in stress or strain is termed *anelastic relaxation*. Anelastic relaxation is characterised by a *relaxation strength* Δ and by distribution of *relaxation times* τ. In the case of applied constant stress relaxation strength can be defined as $\Delta = (\varepsilon_R - \varepsilon_U)/\varepsilon_U$ or expressed through compliance $\Delta = (J_R - J_U)/J_U$. Stress relaxation can be expressed also as $\Delta = (M_U - M_R)/M_R$, where indexes U and R correspond to unrelaxed and relaxed values.

In the case of cyclic loading the behaviour of the anelastic solid can be described in complex notations:

$$\sigma^* = \sigma_0 \exp(i\omega t), \qquad (1.2-2)$$

where σ_0 is the stress amplitude and ω is circular frequency. Then corresponding strain response can be expressed as:

$$\varepsilon^* = \varepsilon_0 \exp(i(\omega t - \phi)), \qquad (1.2-3)$$

where ε_0 is the strain amplitude and ϕ is the angle of phase lag between stress and strain, which is called the *loss angle*. Then complex modulus, which will be dependent on circular frequency ω can also be defined as:

$$M^*(\omega) = \sigma^*/\varepsilon^* = |M(\omega)|\exp(i\phi(\omega)) = M_1(\omega) + iM_2(\omega), \qquad (1.2-4)$$

where $|M(\omega)| = \sigma_0/\varepsilon_0 = \sqrt{M_1(\omega)^2 + M_2(\omega)^2}$ is *absolute dynamic modulus*, $M_1(\omega)$ is the real part of $M^*(\omega)$, called *storage modulus* and $M_2(\omega)$ is imaginary part of $M^*(\omega)$, called *loss modulus*. Then ratio of loss modulus to storage modulus will define the loss tangent:

$$\tan\phi = M_2/M_1. \qquad (1.2-5)$$

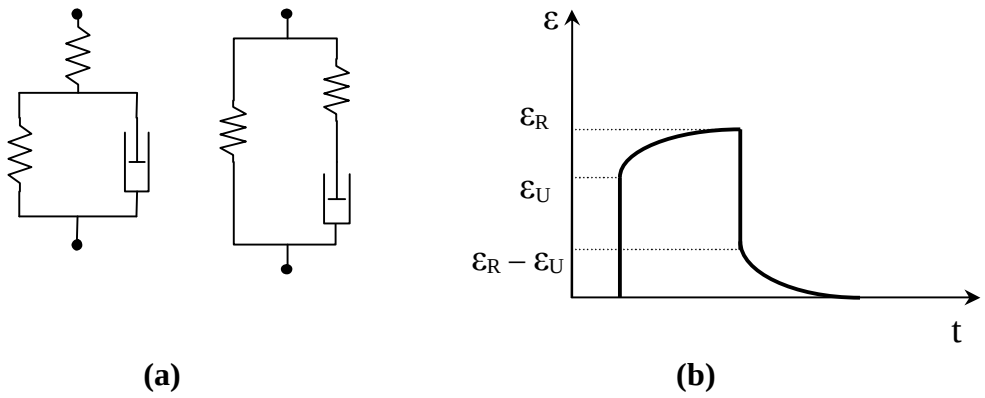

Figure 3. Examples of completely recoverable three-parameter models of standard anelastic solid. (Blanter et al., 2007)

According to Nowick and Berry (1972) the dissipated energy in a full cycle (ΔW) and maximum stored energy (W) per unit of volume equals to:

$$\Delta W = \pi M_2 \varepsilon_0^2 \qquad \text{and} \qquad W = \frac{1}{2} M_1 \varepsilon_0^2 . \qquad (1.2-6)$$

Thus,

$$Q^{-1} = \Delta W / 2\pi W = M_2 / M_1 = \tan\phi . \qquad (1.2-7)$$

The dynamic response functions of the standard anelastic solid are usually given by Debye equations (Nowick and Berry, 1972), which can be written for modulus and internal friction under condition where the relaxation strength $\Delta << 1$ as:

$$M(\omega) = M_R\left(1+\Delta\frac{\omega^2\tau^2}{1+\omega^2\tau^2}\right) = M_U\left(1-\frac{\Delta}{1+\Delta}\frac{1}{1+\omega^2\tau^2}\right) \approx M_U\left(1-\frac{\Delta}{1+\omega^2\tau^2}\right), \qquad (1.2-8)$$

$$Q^{-1}(\omega) = \frac{\Delta}{\frac{1}{\omega\tau}+\omega\tau}, \qquad (1.2-9)$$

where τ is the *relaxation time* of the time dependent process. Most of the known mechanisms of anelastic relaxation are thermally activated processes, related to the motion of various kinds of defects or solute atoms in the crystal lattice of the material. Thus, the value of the relaxation time is dependent on temperature and represents reciprocal relaxation rate or in other words the reciprocal jump frequency of the defects or solute atoms to overcome the energy barrier at a definite temperature. Therefore, the dependency of the relaxation time from temperature can be expressed by reciprocal Arrhenius equation as:

$$\tau = \tau_0 \exp(H / kT), \qquad (1.2-10)$$

where τ_0 is the limit relaxation time or reciprocal attempt frequency, H is the effective activation enthalpy (or apparent activation energy), k_B is the Boltzmann's constant and T is absolute temperature. The Debye peak has its maximum at $\omega\tau = 1$, which value is equal to $\Delta/2$. The equation (1.2 – 10) can be rewritten as:

$$\omega\tau = \omega\tau_0 \exp(H / kT). \qquad (1.2-11)$$

The temperature for the condition of the peak maximum ($\omega\tau = 1$) is defined as:

$$\omega\tau_0 = \exp(-H / kT_m). \qquad (1.2-12)$$

Inserting equation (1.2 – 11) and (1.2 – 12) into (1.2 – 9) gives an equation for the Debye peak as a function of temperature at constant oscillation frequency:

$$Q^{-1}(T) = \frac{\Delta}{e^{-\frac{H}{k}(T^{-1}-T_m^{-1})} + e^{\frac{H}{k}(T^{-1}-T_m^{-1})}} = \frac{\Delta}{2\cosh\frac{H}{k}\left(T^{-1}-T_m^{-1}\right)}. \qquad (1.2-13)$$

The dependencies of dynamic modulus and internal friction of standard anelastic solid with single relaxation time on $\log(\omega\tau)$ and on temperature are shown in Fig. 4. The resulting Debye peak $Q^{-1}(\omega)$ plotted versus $\log(\omega\tau)$, as shown in Fig. 4a, is symmetrical in relation to the peak maximum at $\log(\omega\tau) = 0$ (or $\omega\tau = 1$), with a damping maximum of $\Delta/2$ and with the width of the peak at half maximum of 1.144. The asymptotic behaviour for $\omega\tau \to 0$ and $\omega\tau \to \infty$ implies that at these limits the loss angle is equal to zero and purely elastic behaviour with slopes M_U for $\omega\tau >> 1$ and M_R for $\omega\tau << 1$ is observed. In order to trace the Debye peak reasonably well at constant temperature, as it is seen in Fig. 4a, the frequency ω has to be varied over about four orders of magnitude, while the relaxation time τ may be varied over a wide range of values by changing temperature, as it depends on temperature exponentially (Eq. 1.2 – 10). Therefore, an

internal friction spectra is usually obtained as the temperature dependence of internal friction at nearly constant oscillation frequency. An example of the internal friction peak for the standard anelastic solid with a single relaxation time plotted versus temperature is shown in Fig. 4b. The Debye peak plotted in reciprocal temperature scale is also symmetric in relation to the peak maximum at $1/T_m$, with the width of the peak at half maximum defined as $\Delta(1/T) = 2.635\ k/H$ (Nowick & Berry, 1972). If a series of peaks is obtained at a number of different frequencies, a straight line plot can be made of $\ln\omega$ versus $1/T_m$ using Eq. 1.2 – 12. The slope of this line is equal to H/k and intercept of it with $\ln\omega$ corresponds to $\ln(\tau_0^{-1})$. This method is the most common way to obtain the effective activation enthalpy (or apparent activation energy) and the limit relaxation time for the relaxation process. This is even possible for internal friction peaks which are much broader than a Debye peak, which means that the underlying physical process includes several relaxation times instead of just one. For this case, the activation parameters (H and τ_0) correspond to some average values (Nowick & Berry, 1972).

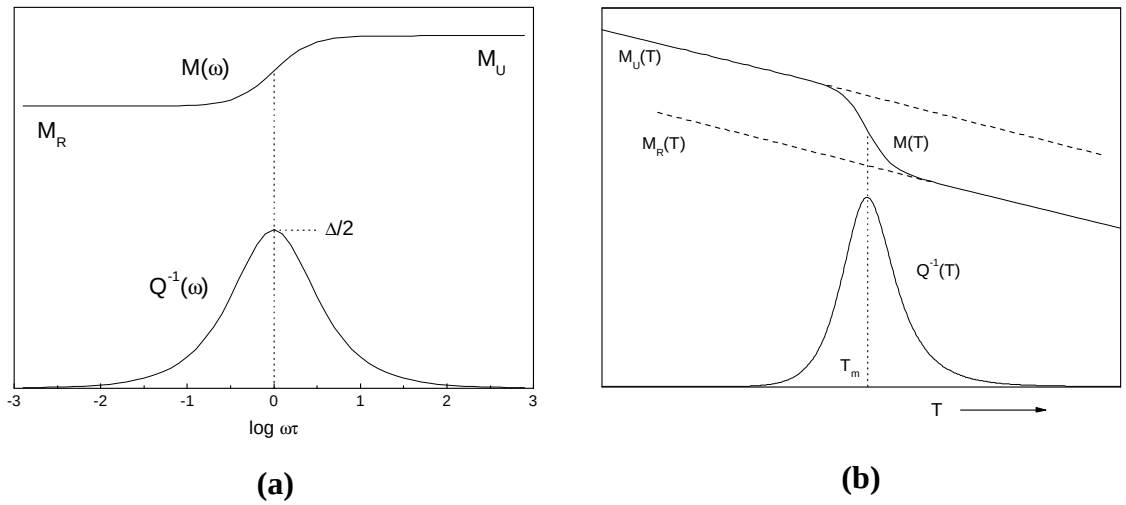

Figure 4. Internal friction (Q^{-1}) and dynamic modulus (M) of the standard anelastic solid plotted as a function of log ($\omega\tau$) at constant temperature (a), and as function of temperature at constant frequency (b).

1.2.2 Snoek relaxation

The Snoek relaxation is an anelastic relaxation caused by interstitial atoms (O, N, C) in the BCC metals and alloys. In BCC metal lattice, the interstitial atoms, such as O, N and C, are usually located in the octahedral sites and result in lattice distortions of tetragonal symmetry oriented along three main lattice directions ([100], [010] and [001]). In the absence of the external stress, the dissolved interstitials are distributed uniformly among the octahedral sites in all the three directions. If a tensile stress is applied along one of the directions, the arrangement of the dissolved interstitials along this direction becomes energetically more favourable and will result in a diffusion of interstitial atoms from the energetically less favourable sites to the more favourable. The change of the stress sign will result in the reverse process. This change in the distribution of interstitial atoms under applied stress causes an anelastic deformation of the crystal associated with a change in lattice spacing along the three main crystal axes.

1.2.3 Snoek-like relaxation in FCC metals and alloys

The original model of the relaxation suggested by Verner in 1965 was based on the mechanism of interstitial-interstitial (*i*-*i*) atom pair re-orientation. This model predicts, in agreement with the experimental data, square and linear dependence of the peak height on interstitial atom concentration, when the concentration is low and high, respectively. Several models have been suggested for this relaxation process based on the re-orientation of interstitial-substitutional (*i*-*s*) atoms and interstitial atom-vacancy (*i*-*v*) pair re-orientation, see the summary in (Blanter et al., 2007). Alternative explanation of Snoek-like peak, suggested by Jagodzinski et al. (1998), assumes that the relaxation is caused by the movement and re-orientation of a single interstitial, which induces in the lattice of stainless steel non-cubic elastic distortions in multicomponent alloys, such as, for example, austenitic stainless steels or Ni-base alloys as the octahedral interstitial sites are non-equivalent due to different combination of substitutional atoms forming the site (Grujicic et al., 1988; Grujicic & Owen, 1995). In multicomponent alloys, interstitial atoms interact differently with the alloying elements.

Thus, the symmetry of the local coordination shells around the interstitial atom can be lower than cubic, giving rise to elastic dipoles.

1.2.4 Hasiguti IF peaks in FCC metals and alloys

The Hasiguti peaks have been found in deformed metals with different crystal lattices (Hasiguti et al., 1962). In FCC metals three Hasiguti peaks have been reported, and they are denoted as P1, P2, and P3 depending on the location of the peak maximum on the temperature scale. The number of Hasiguti peaks observed in the deformed material depends on the deformation conditions (the deformation temperature and its mode). The presence of impurities usually decreases the height of the Hasiguti peaks as a result of dislocation pinning (Blanter et al., 2007). The Hasiguti relaxation was attributed to the processes of dislocation motion in the presence of point defects produced during plastic deformation. The three Hasiguti peaks in FCC metals were attributed to the interaction of dislocations with vacancies (P1), self-interstitials (P2) and divacancies (P3) (Burdett & Queen, 1970).

2 Aims of the study

The aim of this research work was to determine the temperature and strain rate ranges where DSA is promoted in austenitic stainless steels grade 316L and commercial Ni-base Alloy 600 and Alloy 690. It was also aimed to examine and compare the DSA manifestations and its influence on the mechanical properties of 316 austenitic stainless steel with different contents of nitrogen and Ni-base alloys Alloy 600 and Alloy 690. Another aim was to determine the differences in the resulting dislocation structures and internal friction response of the materials pre-strained under conditions promoting and not promoting the DSA behaviour. An understanding of the diffusion of interstitials in solid solution, especially in stress fields, is essential in order to determine, which of the several possible mechanisms are responsible for DSA in the studied materials. Therefore, it was important to obtain the activation enthalpies of the close range diffusion of carbon and nitrogen in the studied austenitic stainless steels and Ni-base alloys.

3 Materials and experimental

3.1 Materials

Several industrial and model laboratory materials were selected for the present study. A detailed description and the history of the materials are presented in Publications I, II and V. The chemical compositions of the studied materials are summarized in Tables 2 and 3.

Table 2. Chemical compositions of the studied austenitic stainless steels

Type	Code	Fe	Ni	Cr	C	N	Mo	Mn	Al	Cu	Si
316LN	1042	bal.	11.0	16.8	0.022	0.028	2.1	1.5	0.02	0.20	0.51
316LN	1043	bal.	11.1	16.8	0.022	0.085	2.0	1.5	0.02	0.19	0.52
316LN	1045	bal.	11.2	17.0	0.022	0.176	2.1	1.5	0.02	0.18	0.53
316NG	BB44	bal.	12.5	17	0.022	0.093	2.28	1.66	0.01	0.11	0.38

Table 3. Chemical compositions of the studied Ni-base alloys

Type	Code	Fe	Ni	Cr	C	Ti	Co	Mn	Al	Cu	Si
Alloy 600	7216 H	8.1	bal.	16.1	0.04	0.16	0.29	0.22	0.17	0.01	0.32
Alloy 690	6030	8.4	bal.	27.7	0.01	0.14	0.07	0.22	0.18	0.01	0.23

3.2 Experimental

3.2.1 Optical metallography

Optical microscopy was employed for the evaluation of grain size. The samples for optical microscopy were cut from the bulk materials in as-supplied state by an abrasive disc saw and then mechanically wet ground with SiC emery paper up to 2500 grit. The

final polishing was performed using 5 μm and finishing with 1 μm diamond paste. In order to reveal the grain structure two different etchants were used. For austenitic stainless steels electrolytic etching at 1.0 V at room temperature for about 5 min in solution of 60 ml of nitric acid in 40 ml of distilled water was utilized. Samples of Ni-base alloys were etched for 2 min in Kallings no. 2 etch solution (2 g $CuCl_2$ – 40 ml HCl – 60 ml ethanol) at room temperature. The samples were studied with Nikon Epiphot 200 optical microscope.

3.2.2 Tensile tests

All tensile test specimens were fabricated according to the ASTM standard E8M (sheet-type sub-size specimens), with the gauge length of 32 mm, thickness of 2 mm and width of 6 mm. Tensile tests were performed according to the standards SFS-EN 1002-1 and ASTM E21 (Standard Test Method for Elevated Temperature Tension Tests of Metallic Materials) in air environment. Tensile tests were carried out using a 25 kN MTS 858 test machine equipped with a MTS High-Temperature Furnace 653.02 at strain rates in the range of 10^{-3} - 10^{-6} s^{-1} and temperatures from 100 to 800 ^{o}C. The strain rate sensitivity was measured using step-wise changes of the strain rate from 10^{-4} to 10^{-6} s^{-1} and in the reverse way during tensile testing, with the ratio of initial and subsequent strain rate ($\dot{\varepsilon}_1 / \dot{\varepsilon}_2$) equal to 100 or 0.01. To calculate the strain rate sensitivities in true stress – true strain coordinates a linear interpolation of each strain rate interval was performed. The step-wise tests were performed at 200, 288 and 400 ^{o}C for 316NG austenitic stainless steel and at 100, 200 and 300 ^{o}C for Ni-base Alloy 600 and Alloy 690.

3.2.3 Internal friction method

The internal friction (IF) method was used to determine the presence of the free nitrogen and carbon and their diffusive redistribution in the crystalline lattice of the studied materials. Specimens of 316NG austenitic stainless steel for IF measurements were

taken from the gauge lengths of tensile test specimens strained to 20 % elongation at the strain rate of 10^{-5} s^{-1} and at the temperatures of 200, 288 and 400 ^{o}C. The IF specimens of Alloy 600 and Alloy 690 were taken from tensile test specimens strained to about 50 % elongation at the strain rate of 10^{-5} s^{-1} and temperatures of 100, 200 and 300 ^{o}C. The cooling time to RT after the straining at elevated temperatures did not exceed 2 min for all samples used for further IF measurements. The specimens had the typical dimensions of 0.5 × 1.5 × 45 mm, which were prepared by cutting with a water-cooling abrasive disc saw and then mechanically polishing with 1200 grit emery paper.

The temperature dependencies of the internal friction, Q^{-1}, were measured using the method of free decay of resonance oscillation by an inverted torsion pendulum over the temperature range from RT to 500 °C with the amplitudes of the torsion deformation less than 10^{-5}. The natural frequency of the pendulum was ~1.5 Hz. The heating rate was kept at 2 °C/min.

3.2.4 Transmission electron microscopy

TEM examinations were performed only for AISI 316NG austenitic stainless steel. Specimens for TEM examination were prepared from the deformed gauge region of the tensile specimens tested to fracture at the strain rate of 10^{-5} s^{-1} and temperatures of 200 and 400^{o}C. The cooling time of the tensile specimens to RT after the straining at elevated temperatures did not exceed 2 min. Part of the gauge length of the tested tensile specimens were first ground to about 0.1 mm thickness, and then 3 mm diameter disk specimens for TEM were punched from the gauge length. The disks were subsequently electropolished to electron transparency with a Tenupol 5 running a 3% perchloric acid/methanol solution at -35 ^{o}C and 23-26 V.

4 Results

4.1 Mechanical manifestations of DSA

Manifestations of DSA by serrated flow and negative strain rate sensitivity for studied materials are shown in Figs. 5 – 7. The development of serrated flow with temperature in the tensile test conducted at the strain rate of 10^{-5} s^{-1} for AISI 316NG austenitic stainless steel is shown in Fig. 5a. The tensile tests revealed that in AISI 316NG austenitic stainless steel serrated flow is well-defined at the testing temperatures from 288 to 500 ^{o}C, while at 200 ^{o}C and above 600 ^{o}C serrated flow was not observed. At 288 ^{o}C only periodic abrupt changes in stress, which correspond to serrated flow of type A were present on the stress-strain curve. In the test conducted at 400 ^{o}C, the amplitude of the serrations increased with strain and they changed in series from A to A+B type, and at higher strain values, to mainly B-type serrations, which are oscillations around the general level of the stress-strain curve occurring in quick succession. At 500 ^{o}C only B-type serrations were observed. Dependencies of the strain rate sensitivity on the temperature of the step-wise tensile test and on flow stress for AISI 316NG steel are shown in Fig. 5b. The results obtained for strain rate sensitivity correlate with the development of serrated flow. At 200 ^{o}C, where serrations are not observed on stress-strain curve, the strain rate sensitivity remains positive for all the values of flow stress. At 288 ^{o}C, where only serrations of type A were observed, the strain rate sensitivity was about zero with minor deviations to negative values at flow stresses over 400 MPa. At 400 ^{o}C, where the serrated flow is well developed and the amplitude of the serrations is maximal, the strain rate sensitivity had negative values already at 200 MPa and was decreasing with increasing flow stress.

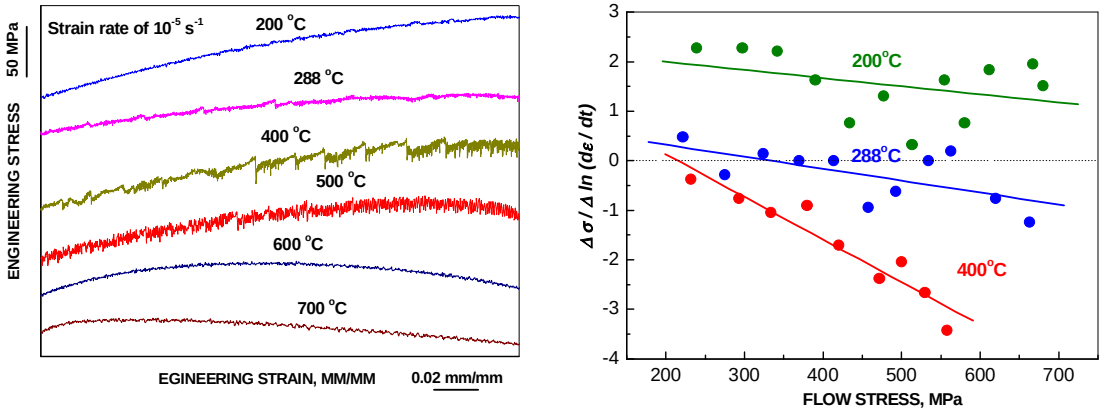

(a) **(b)**

Figure 5. Manifestations of DSA in AISI 316NG austenitic stainless steel in engineering stress-strain curves obtained at strain rate of 10^{-5} s^{-1} at different temperatures (a) and in the dependencies of strain rate sensitivity on flow stress obtained from step-wise tests at strain rates of 10^{-4} and 10^{-6} s^{-1} (b). (Publication II)

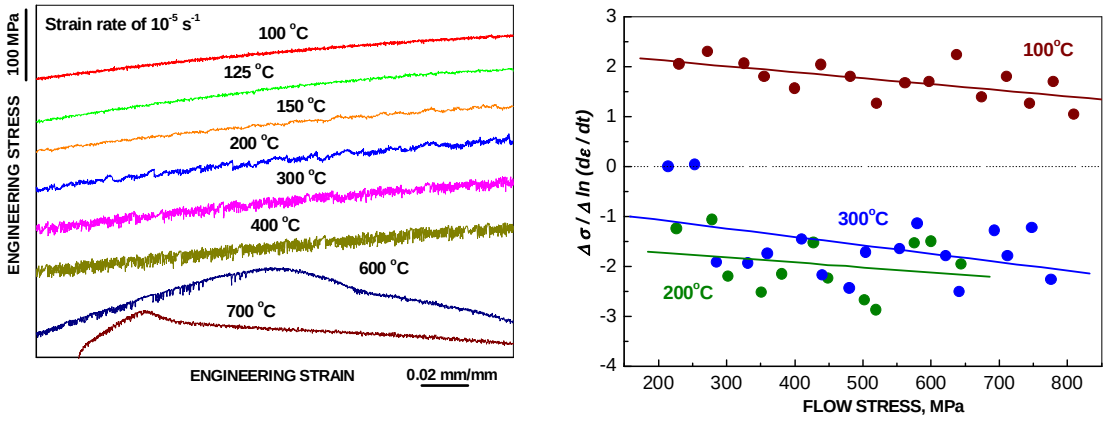

(a) **(b)**

Figure 6. Manifestations of DSA in Alloy 600 in engineering stress-strain curves obtained at strain rate of 10^{-5} s^{-1} at different temperatures (a) and in the dependencies of strain rate sensitivity on flow stress obtained from step-wise tests at strain rates of 10^{-4} and 10^{-6} s^{-1} (b). (Publication V; Ivanchenko et al., 2009)

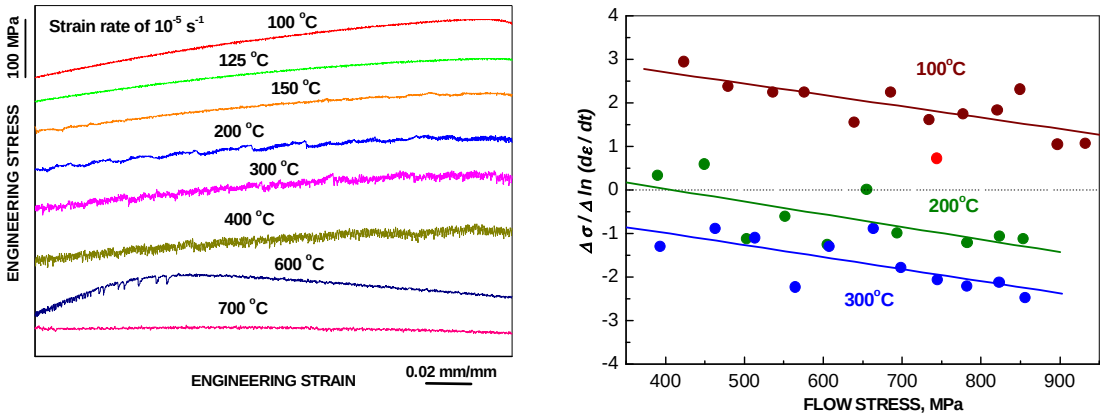

(a) **(b)**

Figure 7. Manifestations of DSA in Alloy 690 in engineering stress-strain curves obtained at strain rate of 10^{-5} s^{-1} at different temperatures (a) and in the dependencies of strain rate sensitivity on flow stress obtained from step-wise tests at strain rates of 10^{-4} and 10^{-6} s^{-1} (b). (Publication V; Ivanchenko et al., 2009)

The temperature range, where the serrated flow is observed, is wider for Alloy 600 and Alloy 690 than for AISI 316NG steel, strained at the same strain rate of 10^{-5} s^{-1}. Serrated flow of type A becomes well recognised in the stress-strain curves obtained at the strain rate of 10^{-5} s^{-1} already at 150 °C for Alloy 600, Fig. 6a, and at 200 °C for Alloy 690, Fig. 7a. At 300 and 400 °C serrated flow changes to B-type and at 600 °C to type C for both studied Ni-base alloys. The measurements of strain rate sensitivity for these alloys are shown in Figs. 6b and 7b. As can be seen from Figs. 6 and 7, positive strain rate sensitivity values correspond to deformation conditions where smooth flow was observed. At 200 and 300 °C serrated flow appears on stress-strain curves and strain rate sensitivity values become negative. The simultaneous observation of serrated flow and negative strain rate sensitivity is a clear confirmation of DSA phenomenon in the studied materials.

The dependencies of the onset of serrations in 316NG steel, Alloy 600 and Alloy 690 on temperature and strain rate are shown in Fig. 8. The data summarises the appearance of serrations in the stress-strain curves of the studied materials at different strain rates and testing temperatures. In the case of filled data points DSA serrations take place while

open ones mean that no serrations were observed. The dotted lines in Fig. 8 represent the critical strain rate as a function of testing temperature for DSA occurrence. This dependence is widely used for the calculation of activation energy of DSA occurrence and it can be expressed as

$$\dot{\varepsilon}_c = \dot{\varepsilon}_c^0 \exp\left(-\frac{H}{k_B T}\right), \qquad (4.1-1)$$

where $\dot{\varepsilon}_c^0$ is a pre-exponential factor, k_B and T is Boltzmann's constant and temperature, respectively, H is representing the apparent activation energy of the DSA occurrence. The enthalpies for the onset of DSA calculated from the dotted lines in Fig. 8 are about 1.2 eV for 316NG steel and about 1.6 eV for both Ni-base alloys. The boundary for the Alloy 600 is at lower temperatures as compared to that of the Alloy 690.

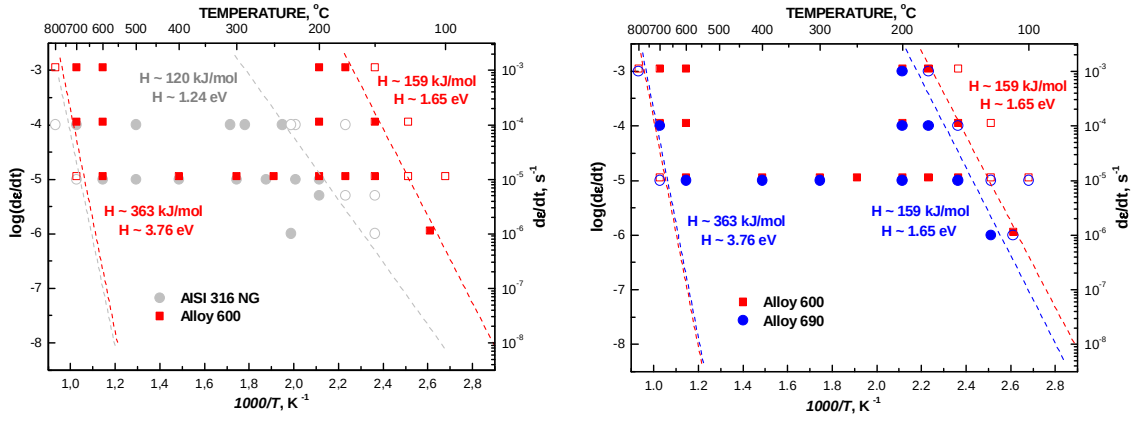

Figure 8. Comparison maps of the serrated flow appearance depending on temperature and strain rate for AISI 316NG steel and Alloy 600 shown by grey circles and red squares, respectively (a), and for Alloy 600 and Alloy 690 shown by red squares and blue circles, respectively (b). Filled data points correspond to strain rate and temperature values at which serrated flow occurs in stress-strain curves and open points correspond to smooth flow. The dashed lines are the boundaries for the onset (or disappearance) of serrations. (Publication II; Publication V; Ivanchenko et al., 2009)

4.2 Analysis of the measured stress-strain curves by FFT

The A-type serrations observed in the studied AISI 316 stainless steels correspond to quasi-regular separate pulses of flow stress and the average time between the pulses can be obtained by using Fourier transformation of the oscillating flow stress as a function of time. Fourier spectra of DSA serrations observed in the stress-strain curves of AISI 316NG steel measured at the strain rate of 10^{-5} s^{-1} at the studied temperatures are shown in Fig. 9. At the testing temperature of 200 ^{o}C, where no serrations were observed, Fourier spectrum of the flow stress signal represents only a random noise of dynamometer and it is a monotonic decreasing function of frequency. In the presence of quasi-regular serrations in the stress-strain curve, as it can be seen at 288 and 400 ^{o}C in Fig. 9, some maxima arise in the Fourier spectra. The maxima shown by arrows correspond to separate pulses which reflect the repeated advancement of the Lüders band through the specimen. The average time between pulses at 400 ^{o}C was estimated to be 2.83 ks.

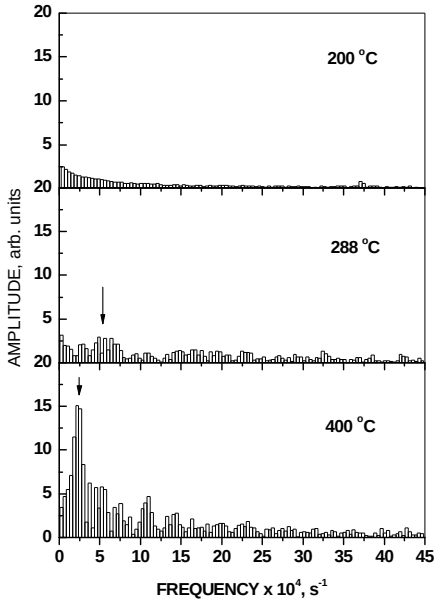

Figure 9. Fourier transformation spectra of the flow stress signal in the tensile tests of AISI 316NG stainless steel at the strain rate of 10^{-5} s^{-1} and at different temperatures. Arrows correspond to quasi-regular separate pulses. (Publication I)

Fourier spectra of DSA serrations observed in the stress-strain curves of Alloy 600 and Alloy 690 tested at the strain rate of 10^{-5} s^{-1} in the temperature range of 100 to 400 ^{o}C are shown in Fig. 10. It can be seen that at 100 ^{o}C the Fourier spectrum of the flow stress signal represents only random noise. In the presence of quasi-regular serrations of type A in the stress-strain curve at 200 ^{o}C low frequency maxima shown by arrows and denoted by 1 in Fig. 10 arise in the Fourier spectra of both Ni-base alloys. Application of the Gaussian distribution to maxima in the low frequency part of Fourier spectra gives a modal value of frequency around 5.5×10^{-4} Hz for Alloy 600 and 6.0×10^{-4} Hz for Alloy 690 corresponding approximately to 1.8 ks and 1.7 ks, respectively. These two characteristic times reflect the repeated advancement of the Lüders band through the specimen. It can also be seen in Fig. 10 that high frequency maxima, which correspond to type B serrations and are denoted by 2 in Fig. 10, arise in the Fourier spectra with the temperature increase.

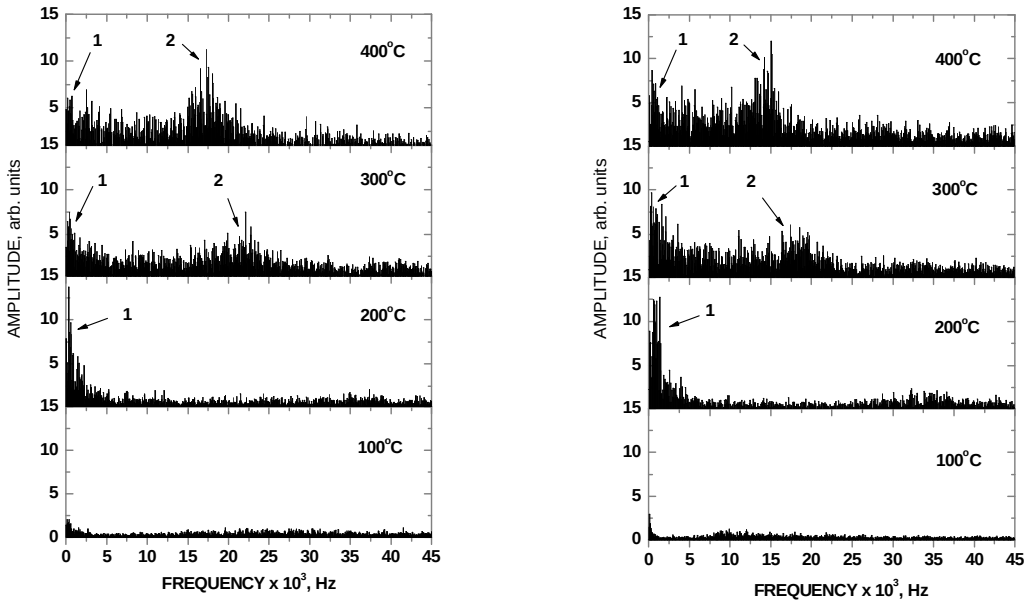

Figure 10. Fourier transformation spectra of the flow stress signal in the tensile tests of Alloy 600 (a) and Alloy 690 (b) at the strain rate of 10^{-5} s^{-1} and at different temperatures; number 1 corresponds to low frequency maxima and 2 to high frequency maxima. (Publication V)

4.3 Microstructural manifestations

TEM examination of AISI 316NG steel presented in Fig. 11 reveals the differences in dislocation sub-structures of the steel strained at two different temperatures at the strain rate of 10^{-5} s^{-1}: 200 ^{o}C, where smooth flow was observed; and 400 ^{o}C, while DSA was manifested by jerky flow of type A+B. As shown in Fig. 11a, the microstructure in the material following tensile testing at 200 °C was comprised of small, thick-walled cells. Cellularization is a result of mutual annihilation of dislocations, and the reorganization of remaining dislocations into a lower energy structure. It is enabled by cross-slip, i.e. dislocation glide on multiple planes simultaneously. As shown in Fig. 11b, the microstructure following tensile testing at 400 °C showed much more linearity than that at 200 °C. That is a consequence of dislocation glide occurring on particular planes. According to DSA theory, the interaction between dislocations and solute atoms limits the freedom of motion of the dislocations; i.e. by pinning portions of the dislocations, the ability of the dislocations to cross-slip is restricted. That produces planar slip, which is manifested as linear microstructures.

A comparison of the microstructures of the samples strained at 200 and 400 °C reveals some differences. In particular, the material tensile tested at 400 °C showed a greater tendency towards dislocation planarization, manifested as highly linear dislocation structures. Corresponding tensile test and internal friction measurements also showed serrations on the tensile stress-strain curve and a clearly increased Snoek-like peak height, respectively. On the other hand, the steel tensile tested at 200 °C did not have such straight dislocations, nor did it show serrated flow, while the Snoek-like peak was not as high as that for 400 °C. Thus, it appears that the planarization in the dislocation microstructure correlates with the IF results, and both are correlated with the observed altered tensile stress-strain behavior.

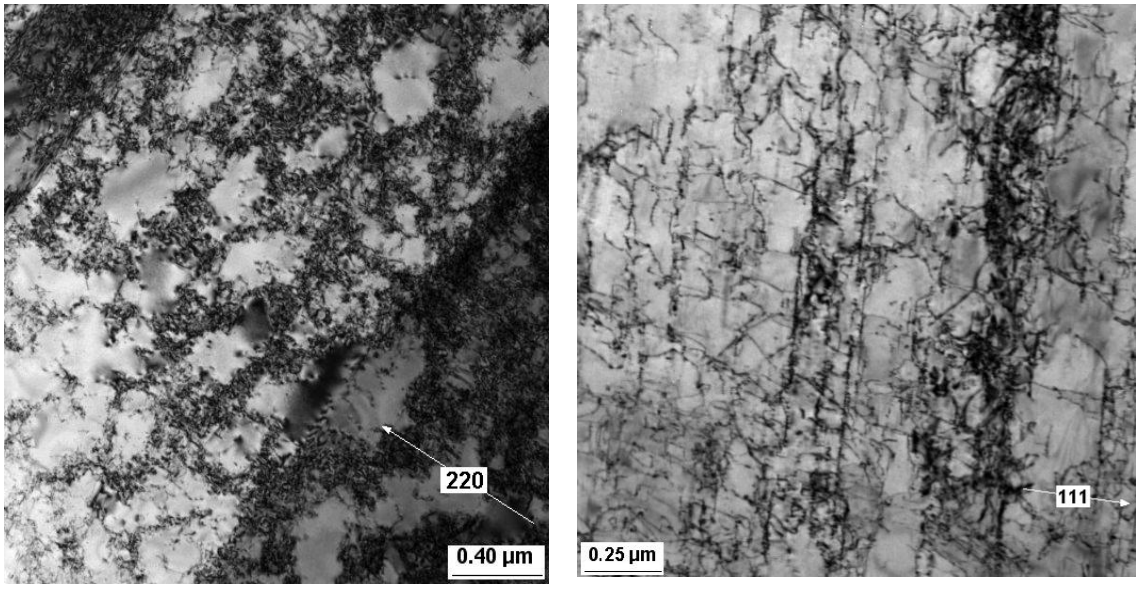

(a) **(b)**

Figure 11. TEM examination of AISI 316NG steel strained to fracture at the strain rate of 10^{-5} s^{-1}. The microstructure is studied in the gauge region following tensile testing at 200 ^{o}C (beam is parallel to [100]) (a), and at 400 ^{o}C, which shows much more linearity than that at 200 ^{o}C (beam is parallel to [110]) (b). Arrows indicate g-vectors. (Publication III)

4.4 Influence of DSA on mechanical properties

From the measured temperature dependencies of yield strength, ultimate tensile strength (UTS), elongation to fracture and strain hardening coefficient shown in Fig. 12, one can observe that yield strength decreases with testing temperature with rather constant decline as DSA was observed in 316 stainless steel, while in the studied temperature range of 200 – 400 ^{o}C UTS seems to be affected and remains almost constant due to the increase of strain hardening coefficient with temperature. This result corresponds to the plateau on the temperature dependence of the ultimate tensile strength observed in (Kim et al., 1998) for 316LN steels in the DSA temperature range. As a function of temperature, the elongation to fracture varies only by 2-4 %. Rather similar dependencies of mechanical properties on temperature were observed for commercial Ni-base alloys Alloy 600 and Alloy 690. The results of DSA manifestation in

mechanical properties for the Ni-base alloys are presented in Fig. 13. Yield strength and ultimate tensile strength decrease with increasing testing temperature up to 200 ^{o}C and remain constant after that, Figs. 13a and b. The strain hardening coefficient increases with increasing testing temperature up to 200 ^{o}C, while it is almost constant above 200 ^{o}C for both studied alloys, Fig. 13c. As a function of temperature, the elongation to fracture increases for both Ni-base alloys except for Alloy 600 at 400 ^{o}C a decrease of ductility is observed, Fig. 13d.

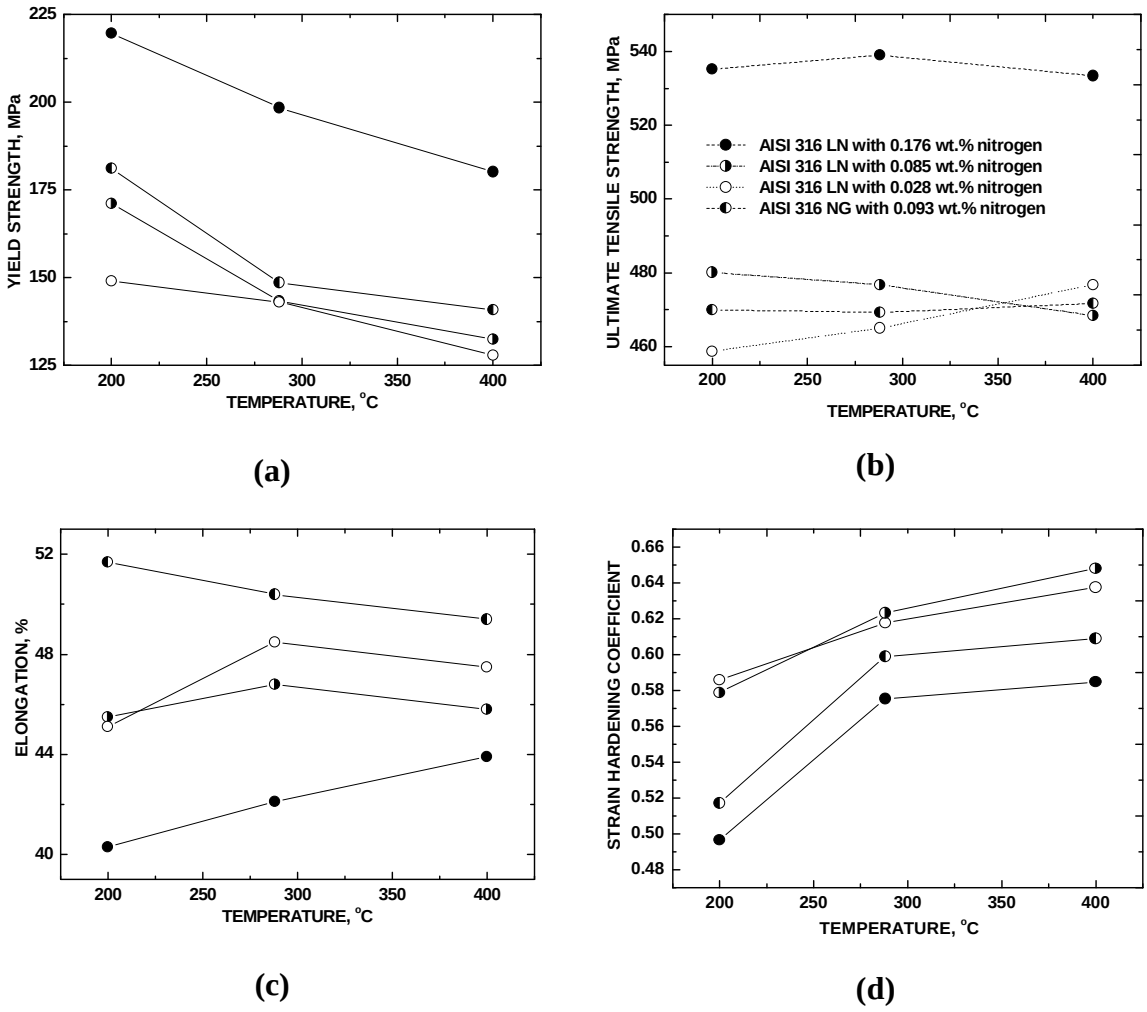

Figure 12. Temperature dependencies of yield strength (a), ultimate tensile strength (b), elongation to fracture (c) and strain hardening coefficient (d) for the studied stainless steels. Symbols defined in (b) apply for all pictures. (Publication II)

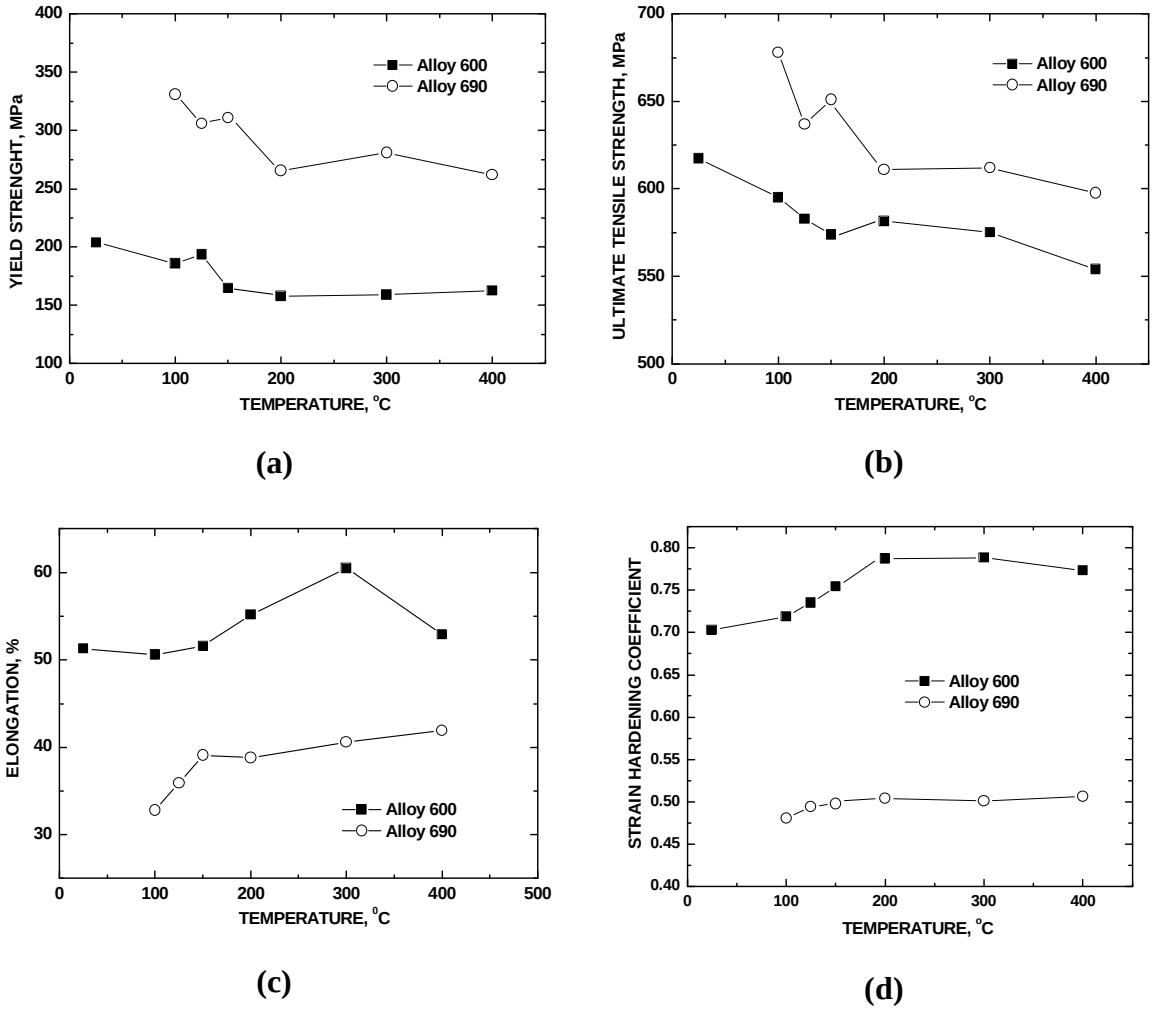

Figure 13. Temperature dependence of yield strength (a), ultimate tensile strength (b), elongation to fracture (c) and strain hardening coefficient (d) of the studied Alloy 600 and Alloy 690 obtained at the strain rate of 10^{-5} s^{-1}. (Publication V)

4.5 Effect of nitrogen alloying

Nitrogen alloying increases the strength of 316L stainless steels in the testing temperature range and the elongation to fracture decreases with increasing nitrogen content except in the case of the commercial 316NG stainless steel, which demonstrates highest elongation to fracture in the whole range of testing temperatures. Results obtained in the present investigation are in well accordance with previous study (Kim et al., 1998) of nitrogen effects on DSA in 316 stainless steels.

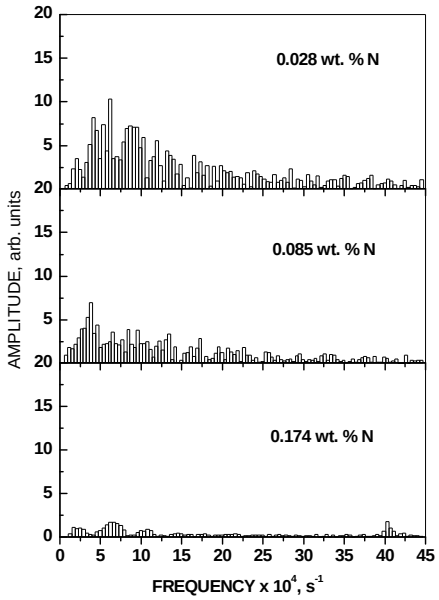

Figure 14. Fourier transformation spectra of the flow stress signal in the tensile tests of AISI 316LN alloys at a strain rate of 10^{-5} s^{-1} and 288 °C. (Publication I)

Influence of the nitrogen content of AISI 316L steel on the Fourier spectra of DSA serrations is shown in Fig. 14. The steels were tensile tested at the temperature of 288 ^{o}C and strain rate of 10^{-5} s^{-1}. It can be seen that nitrogen alloying suppresses markedly the amplitude of DSA serrations in the whole range of frequency. High amplitude irregular pulses of the flow stress observed in the steel with 0.028 wt.% of nitrogen become smaller and quasi-regular with average time between pulses being about 1.53 ks, when the nitrogen content of the steel increases to 0.176 wt.%.

4.6 Effect of prior deformation

Industrial AISI 316NG stainless steel was tensile tested after prior tensile deformation of 5 and 20 % at room temperature. Pre-straining at room temperature leads not only to an increase of yield and ultimate tensile strength values, but it reduces also the onset deformation of DSA. It seems that cold working facilitates the DSA development in

AISI 316NG steel. DSA serrations become visible on the stress-strain curve obtained at testing temperature of 200 °C after 5 % pre-straining.

4.7 Effect of pre-strain at different temperatures on the distribution of interstitial atoms

The temperature dependencies of internal friction of AISI 316NG austenitic stainless steel are shown in Fig. 15, for both the as-supplied state and following the pre-straining (20 %) at 26, 200, 288 and 400°C.

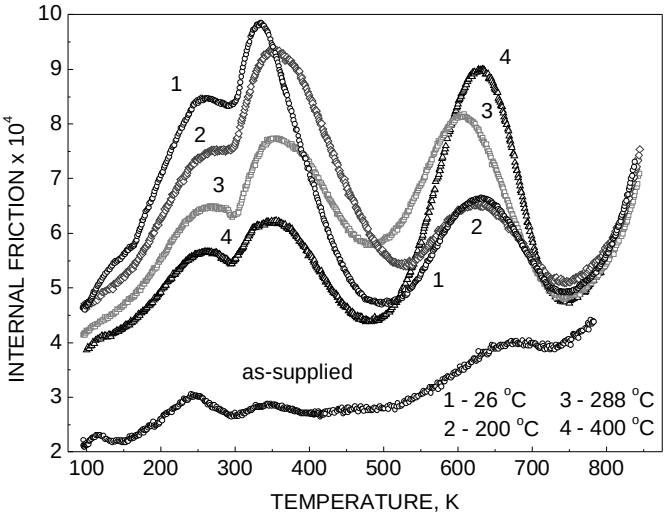

Figure 15. The dependence of internal friction dependencies on temperature for the AISI 316 NG steel after pre-straining (20 %) at different temperatures. (Publication III)

Three well-defined maxima in the Q^{-1} value are apparent for the strained materials, forming peaks located at about −50, 100 and 350°C, while only minor fluctuations were evident for the as-supplied material at the corresponding temperatures. The two lower temperature maxima in the Q^{-1} value (at −50 and 100°C) generally markedly increase in magnitude with the amount of prior cold deformation (Publication I), and were also observed in AISI 310, AISI 304 and interstitial-free AISI 316L austenitic stainless steels

(Publication IV). They are typically considered to be a consequence of an anelastic response of dislocations interacting with point defects induced by cold deformation. The origin of these peaks was analyzed in detail in Publication IV. It was concluded that the IF peak observed in the vicinity of -50 ^{o}C has relaxation origin with the values of activation enthalpy and the pre-exponential factor of the relaxation time of 46 ± 5.8 kJ/mol and $10^{-11\pm1}$ s, respectively, and that it is related to Hasiguti type relaxation. The IF peak with maximum in vicinity of 100 ^{o}C has transitional origin and is probably related to the annihilation of point defects introduced by the plastic deformation at the dislocation cores.

The IF peak observed in AISI 316NG austenitic SS and Ni-base Alloy 600 with its maximum in the vicinity of 350 ^{o}C was recognized to be a result of a Snoek-like relaxation process (Publications I, VI). This relaxation process is induced by the re-orientation of interstitial atoms in the FCC lattice of austenitic stainless steels under periodically applied external stresses originally reported by Rosin and Finkelshtein (1953) and was confirmed by numerous authors in different FCC alloys and pure metals (Blanter et al., 2007). It has been established that the height of the Snoek-like peak is proportional to the concentration of the interstitial atoms in the solid solution of the steels with FCC lattice (Verner, 1965). The peak height and its temperature position may vary depending on the chemical composition of the FCC alloys and they also depend on the distribution of interstitial atoms in the lattice. The corresponding studies and the model for this phenomenon were presented by Jagodzinski et al. (1998) and Yagodzinskyy et al. (2009). The model suggested in these works was used to explain the absence of Snoek-like peak in Inconel 690 alloy, while the DSA phenomenon was manifested (Publication VI).

The activation enthalpies of nitrogen diffusion in FCC lattice of AISI 316NG steel (140 kJ/mol) and the activation enthalpy of carbon diffusion in the lattice of Alloy 600 (162 kJ/mol) obtained by IF method are in good agreement with the apparent enthalpies of DSA occurrence (Publications I, VI). The observed correspondence of the activation enthalpies verifies that the appearance of the DSA results from the interaction of the

free interstitial atoms (C and N) in the solid solution of the materials with mobile dislocations.

To study the influence of DSA on the re-distribution of carbon in Alloy 600 and nitrogen in AISI 316NG austenitic SS, three different regimes of prior deformation at elevated temperatures were applied. For the first regime, the temperature of prior plastic straining was selected below the DSA occurrence, which is 100 ^{o}C for Alloy 600 and 200 ^{o}C for 316NG austenitic SS. For the second regime, temperature was selected in the way that the DSA was manifested by serrated flow of type A (200 and 288 ^{o}C for the Alloy 600 and 316NG austenitic SS, respectively). The third regime represents deformation under the DSA conditions, when the jerky flow of type B was observed. It corresponds to 300 ^{o}C for Alloy 600 and 400 ^{o}C for 316NG austenitic SS.

316NG austenitic SS and Alloy 600 show similar evolution of Snoek-like peak after the prior deformation at elevated temperatures. Temperature dependencies of the internal friction of AISI 316NG austenitic SS and Alloy 600 with different prior deformation procedures are shown in Fig. 16.

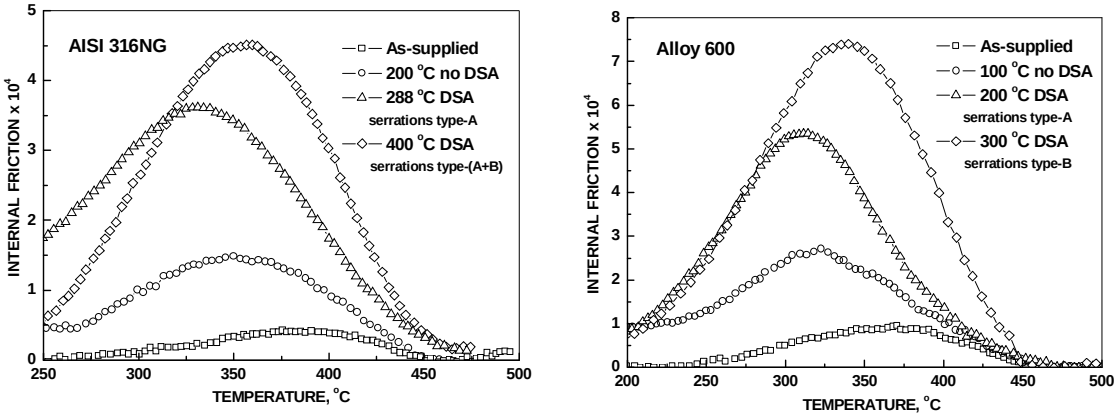

(a) **(b)**

Figure 16. The influence of pre-straining at different temperatures with strain rate of 10^{-5} s^{-1} on the evolution of the Snoek-like internal friction peak in AISI 316NG austenitic stainless steel strained to 20% of elongation (a) and in Alloy 600 strained to 50 % of elongation (b). The background is subtracted. (Ivanchenko et al., 2009)

Well-defined maxima in the internal friction spectra are already apparent for the studied alloys in as-supplied condition. Pre-straining of the materials at elevated temperatures, which do not induce the DSA, increases the height of the Snoek-like peak in both studied alloys by about 3.5 times in relation to the corresponding as-supplied condition values. The influence was even greater after the prior deformation at temperatures, where the serrated yielding attributed to the DSA was observed. Prior deformation under the DSA condition manifested by serrated flow of type A led to more than seven-fold increase in the peak height. The peak height was further elevated (about 10-fold increase) after the pre-straining of the studied materials at temperatures, which induce the DSA serrations of type B.

The enhanced Snoek-like peaks obtained after pre-straining under DSA conditions are unstable. The peak amplitude decays with annealing at the peak temperature as shown in Fig. 17. In the initial stage (about 20 min), the peak annealing process can be described by an elemental exponential decay function (shown by dashed lines in Fig. 17) with the characteristic decay time of 0.92 ± 0.07 ks and 0.95 ± 0.07 ks for Alloy 600 and AISI 316NG austenitic SS, respectively.

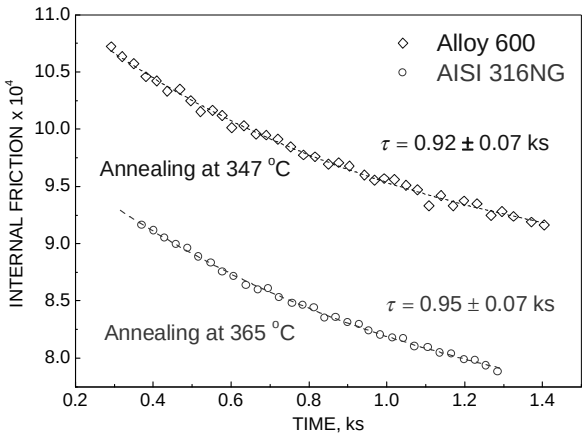

Figure 17. The decay of the Snoek-like IF peak amplitude with annealing time at 347 and 365 ^{o}C for Alloy 600 and AISI 316NG austenitic stainless steel, respectively. The decays are well described by exponential decay function with characteristic times τ shown in the plot. (Ivanchenko et al., 2009)

5 Discussion

The results obtained in the present investigation are in good agreement with literature data on DSA manifestations in austenitic stainless steels and Ni-base alloys. A map of DSA, shown in Fig. 8, summarises the serrated flow appearance in AISI 316NG stainless steel and Ni-base Alloy 600 and Alloy 690 at different strain rates and testing temperatures. In Fig. 8, the dashed lines form the boundaries for temperature and strain rate ranges where DSA occurs. The activation enthalpy values calculated from $\log(\dot{\varepsilon})$ vs $1/T$ dependencies of serrated flow onset using Eq. 4.1 – 1 are about 120 kJ/mol for AISI 316NG austenitic stainless steel and 159 kJ/mol for Alloy 600 and Alloy 690. These values are close to the activation enthalpy of nitrogen and carbon close range diffusion in the crystal lattice of AISI 316NG steel and Alloy 600 obtained by means of internal friction measurements as 140 kJ/mol and 162 kJ/mol, respectively. Thus, it can be concluded that in AISI 316 austenitic stainless steel and Ni-base Alloy 600 within the range of strain rates 10^{-6} – 10^{-4} s^{-1} the diffusion of interstitial atoms (C and/or N) is the rate controlling mechanism of the DSA onset. In principle, this conclusion can be also applied for Alloy 690 despite of the fact that Snoek-like peak was not observed in this alloy. The absence of the IF peak can be explained by two times higher chromium content of Alloy 690 than that of Alloy 600 which increases the amount of octahedral interstitial sites coordinated with six Cr atoms (Grujicic et al., 1988; Grujicic & Owen, 1995). Such interstitial sites have cubic symmetry and can not be involved in the relaxation process, observed as IF peak. Because of the high affinity to chromium, a part of the carbon atoms may be strongly bound to Cr atoms and, therefore, do not induce any measurable anelastic response in Alloy 690.

The great variation in the apparent activation energy of serrated flow appearance that can be found in literature for AISI 316 type steel and Ni-base alloys can be dependent not only on the chemical composition of the alloys and solute atom concentration, but also on the number of other parameters such as testing mode, shape of the specimen, thermal history of the specimen, grain size and the method how activation energy was

derived (Robinson & Shaw, 1994; Rodriguez, 1984; Venkadesan et al., 1992). Thus, rather different results of apparent activation energy for the onset of DSA can be found in literature. The clear effect on IF peak increase in AISI 316NG austenitic stainless steel and Ni-base Alloy 600 after deformation under DSA conditions strongly suggests that interstitial atoms (C or N or both) are involved in the process.

Increase in the IF peak height is related to the atomic re-ordering during plastic deformation and the formation of interstitial enriched sub-micron zones dragged by dislocation pile-ups during the DSA. Similar evolution of the Snoek-like peak with pre-straining at elevated temperatures and nearly the same values of characteristic times of the peak decays suggest the same mechanisms involved in the atomic re-ordering in both AISI 316NG austenitic stainless steel and Ni-base Alloy 600, which occur during the DSA.

Assuming that the Snoek-like peak amplitude is proportional to the nitrogen/carbon concentration in the solid solution, and considering the fact that the pre-straining of the studied austenitic stainless steel results in a remarkable increase in the height of the Snoek-like peak, one can assume that plastic deformation increases the amount of free nitrogen in the steel lattice. There are three possible sources that may provide the free nitrogen in the steel solid solution during plastic deformation: dislocations pinned by nitrogen atoms, grain boundaries with nitrogen segregation, and nitride particles. Because the material of the study was supplied in the annealed condition and with only a minor amount of nitrides, pinned dislocations and nitride particles are unlikely to be a significant source of free nitrogen. Due to the of relatively large grain size, which is about 75 μm, the grain boundaries in the material are estimated to be able to contain no more than about 0.01 wt.% of nitrogen (it is assumed that nitrogen can fully occupy the segregation positions at grain boundaries, the mean atomic portion of which can be estimated as $3h/d$, where $h \approx 1$ nm is the grain boundary thickness and d is the grain size). Nonetheless, its release by plastic deformation cannot account for the observed two-fold increase in the nitrogen peak, considering that the bulk content in the steel is 0.093 wt.%. Thus, some additional mechanism should be taken into account. Additional

relaxation due to re-orientation of *i-i* or *i-s* pairs formed during straining can not be considered as the major mechanisms due to high Cr content of the studied steel (17 wt.%) and transitional nature of the enhanced peak. Also, it is hard to expect peak increase due to the formation of extra *i-v* pairs after the deformation at 288 and 400^{o}C, as the low-temperature IF peaks attributed to point defect-dislocation interactions and annihilation of point defects show opposite behaviour to Snoek-like peak (Publications III, IV).

An alternative explanation for the observed peak increase lies in the Snoek-like peak origin suggested for austenitic stainless steels in (Jagodzinski et al., 1998), and atomic short-range ordering in substitutional alloys (Grujicic et al., 1988; Grujicic & Owen, 1995). In multicomponent alloys, interstitial atoms interact with the alloying elements differently. As a consequence, a octahedral interstitial sites are non-equivalent due to the different combination of substitutional atoms forming the site (Grujicic & Owen, 1995). Thus, the symmetry of the local coordination shells around interstitial atom can be lower than cubic, giving rise to elastic dipoles. Due to their higher affinity to chromium atoms in the austenitic stainless steels, nitrogen atoms prefer to occupy the octahedra with more chromium atoms at the vertices, with the energetically most favourable ones being those with 6 chromium atoms. Interstitial octahedral sites with 6 equivalent substitutional atoms at the octahedron vertices do not take part in the Snoek-like relaxation process, due to the cubic symmetry of the octahedron (Nowick & Berry, 1972). Those interstitial positions of high symmetry shield a part of the nitrogen atoms from the Snoek-like relaxation, with the extent of such shielding depending on the short-range ordering of the substitutional atoms in the steel. This in turn can be characterized by the particular fraction of the octahedra having 6 chromium atoms at the vertices (Jagodzinski et al., 1998; Grujicic & Owen, 1995). The plastic straining of the materials prior to IF measurements changes the substitutional atomic short-range order. This reduces the fraction of high symmetry positions occupied by nitrogen atoms, thereby revealing the presence of the nitrogen interstitials formerly hidden there (Grujicic et al., 1988). That in turn is then manifested as a portion of the increase in the Snoek-like peak height with respect to the annealed condition.

The remaining increase of the peak height following plastic deformation may be a consequence of a long-range re-distribution of nitrogen atoms by dislocation dragging, which results in the formation of nitrogen-enriched zones in the lattice. Such zones are of dynamic origin, forming with the deformation-induced dislocation pile-ups and their re-configurations, and are central to DSA. The enrichment of nitrogen in those zones, which occurs at the expense of the nitrogen atoms coming from the shielded sources, like interstitials in octahedra with 6 Cr atoms, may also increase the fraction of nitrogen atoms taking part in the anelastic relaxation process measured by the IF method.

The nitrogen-enriched zones may occur between dislocation pile-ups, forming dipole-like configurations, where the austenite lattice suffers from a remarkable dilatation. Dynamic trapping of nitrogen to those zones can stabilize the opposite pile-ups, and in turn, it can result in the growth of the pile-ups, which is manifested in TEM-observations as sub-micron scale strain localization having a planar character.

A comparison of the microstructures of the test bars strained at 200, 288 and 400°C reveals some differences. In particular, the material tensile tested at 400°C showed a greater tendency towards the planarization of dislocation structure, manifested as highly linear dislocation structures. That tensile test had also shown serrations in the tensile stress-strain curve, and a clearly increased Snoek-like peak height. The 288°C tensile test showed serrated flow and an increased Snoek-like peak height, and it also resulted in a high proportion of straight, parallel dislocations, though it did not show a long-range planarization observed at 400°C. On the other hand, the 200°C tensile tested material did not have such straight dislocations, nor had it shown serrated flow, while the Snoek-like peak was not as high as that for 288 or 400°C. Thus, it would appear that the planarization in the dislocation microstructure correlates with the IF results, and both are correlated with the altered tensile mechanical behaviour observed. Observed effect of DSA on dislocation structure agrees very well with the results obtained earlier by other authors (Edington & Smallman, 1964; Dingley & McLean, 1967; Michel et al., 1973; Morris, 1974; Kashyap et al., 1988; Kashyap & Tangri, 1997) and confirms the

suggestion of Morris (1974), that the tendency to produce a non-cellular array of dislocations increases with an increase in the intensity of dynamic strain ageing.

There are also other factors which can produce planarity in dislocation structure. For example, low stacking fault energy (SFE) more readily allows separation of dislocations into pairs of partial dislocations, which produces a stacking fault. However, such stacking faults would be readily visible in the microstructure. In these materials stacking faults were only observed in association with the formation of bands of epsilon martensite, which were mainly present only in some grains in the regions associated with a high critical resolved shear stress (especially in the necked region of the tensile test bars). The linearity clearly observed in the dislocation structures at 400°C, and somewhat also at 288°C, in conjunction with the serrations observed in those tensile stress-strain curves and the IF results, would together imply that the mechanism of DSA is controlled by interstitial diffusion at 288 – 400 °C.

The DSA phenomenon is important to the overall deformation behaviour of stainless steel as a contributor to strain localization, as the dislocations pinned by solute atoms have their cross-slip restricted. The restriction of the freedom for cross-slip localizes the strain to the most active slip planes, which produces planar slip. Such a restriction promotes dislocation pile-ups rather than the mutual annihilation of interacting dislocations, which in turn raises the flow stress. Additionally, nitrogen stabilizes dislocation pile-ups and results in additional hardening that is manifested as retardation in the thermally-induced softening generally observed with increasing temperature in stainless steels experiencing DSA. The obtained strain hardening coefficient values are high, especially for the elevated testing temperatures, where DSA serrations are remarkable. In fact, in these conditions, the stress-strain curves do not follow the Hollomon law in the whole plastic strain range. The strain hardening coefficient is highest for the stainless steel with the lowest nitrogen content, in which the DSA serrations are most pronounced.

A suppression of the DSA development in AISI 316LN stainless steel caused by nitrogen alloying looks contradictory as DSA, e.g. in low alloy steels, is enhanced by free interstitials, but it has been already observed before (Kim et al., 1998; 2003; Ganesan et al., 2009). The suppressive effect of nitrogen on DSA may be caused by the increase of the flow stress with nitrogen alloying of the steel causing an increase of the actual stress and consequent possible changes in the deformation response. DSA is expected to result in localisation of plastic deformation to grain boundary regions. This is especially important in cold deformed materials, where DSA was observed to set-on at lower critical strain in all studied grades of AISI 316 austenitic stainless steel. Due to DSA the slow moving dislocations become pinned by solute atmospheres and new dislocations are generated to maintain the strain rate, which results in an increase in the dislocation density and the flow stress. On the same time solute atmospheres restrict dislocation cross-slip and climb, which favors planar slip, which again increases the flow stress. These hardening effects induce increasing stress concentration at the crack tip by preventing the stress relaxation inside the plastic zone, which localizes the strain to the crack tip and increases the crack growth rate, which can explain the effect of DSA in EAC. A detailed explanation of the role of DSA in EAC and the role of deformation as well as composition both of stainless steels and Ni-base alloys need further investigations to reveal the main DSA related parameters affecting EAC.

Conclusions

It was confirmed that DSA occurs in 316 type austenitic stainless steels and Ni-base Alloy 600 and Alloy 690 at temperatures of 300 ^{o}C at wide range of strain rates (10^{-3} – 10^{-6} s^{-1}). It was established that DSA observed in the studied alloys at temperatures around 300 ^{o}C arise from interstitial atom interactions with mobile dislocations.

In spite of the fact that the value of activation energy for DSA onset in Ni-base alloys is higher than that for 316NG austenitic stainless steel, DSA in Alloy 600 and 690 begins at lower temperatures. An apparent activation enthalpy of onset of DSA is about 1.24 eV and 1.65 eV for 316NG stainless and the Ni-base alloys, respectively. The value of the activation energy of DSA onset corresponds well to the enthalpy of nitrogen diffusion in 316NG stainless steel, about 1.45 eV, and the enthalpy of carbon diffusion in Alloy 600 (1.68 ± 0.09 eV) obtained by the internal friction method.

Plastic deformation by straining at temperatures and strain rates relevant for DSA result in an increase in the amplitude of nitrogen-induced Snoek-like IF peak in 316NG austenitic stainless steel and Ni-base Alloy 600. Similar behavior observed for carbon/nitrogen-induced Snoek-like IF peak in the 316NG steel and Ni-base Alloy 600 evidences similar origins of the Snoek-like peak evolution with prior deformation under the DSA conditions for multicomponent substitutional austenitic alloys, regardless of the fact that the IF peak was not detected in Alloy 690. Increase in amplitude of the peak is probably related to atomic re-distribution during plastic deformation and to the formation of interstitial enriched sub-micron zones dragged by dislocation pile-ups during the DSA.

Nearly the same values of characteristic times of the IF peak decays: 0.92 ks for 316NG austenitic stainless steel and 0.95 ks for Alloy 600, correspond to approximately one micrometer diffusion distance and reflect the same mechanism of interstitial re-distribution at the scale of the enriched zones during annealing at the peak temperature.

Deformation microstructures of 316NG austenitic stainless steel, which had been tested under the DSA conditions at temperatures 288^{o}C and 400^{o}C and when the DSA is not observed at 200^{o}C, revealed that long-range planarity was observed in the dislocation structures at 400°C, and short-range planarity at 288°C, but at 200°C the dislocation microstructure was cellular.

It has been found that nitrogen suppresses the serrated flow development in nitrogen alloyed 316L type stainless steels. The onset deformation of serrated flow shifts to higher values of strain and the amplitude of the flow stress pulses decreases with increasing nitrogen content, which can be caused by nitrogen atoms accumulation on dislocations or some dislocation configurations that precedes Lüders band propagation as an elemental DSA event.

IF peak with two well-defined components, which depend on the amount of plastic deformation, is observed in all the studied grades of austenitic stainless steels. The low-temperature component of the observed peak has relaxation origin with similar characteristics to Hasiguti peaks and, thus, is assumed to represent dislocation – point defect interactions. The high-temperature component of the studied peak has transitional origin and is probably related to the annihilation of vacancies formed during the plastic deformation and their diffusion to the dislocation cores. This conclusion is supported by results obtained from positron annihilation spectroscopy (PAS), which has shown a decrease at least to the half in the amount of vacancies after annealing at 500 K.

Pre-straining at room temperature decreases the onset temperature and strain of DSA in 316NG stainless steel. Pre-straining also increases the susceptibility of non-sensitized 316NG stainless steel to intergranular stress corrosion cracking in BWR NWC environment. However, the crack growth rate was found to be lower than that for the sensitized stainless steel.

References

Agarwala, R.P., Naik, M.C., Anand, M.S. & Paul, A.R. 1970. Diffusion of carbon in stainless steels. Journal of Nuclear Materials. Vol. 36:1. pp. 41-47.

Angeliu, T. 2001. Microstructural characterization of L-grade stainless steels relative to the IGSCC behavior in BWR environments. Corrosion 2001. NACE, Houston, Texas. 11-16.03.2001. Paper No 01121, 14 p.

Askill, J. 1967. A bibliography on tracer diffusion in metals. Supplement II. Part I. Self-diffusion in pure metals. Part II. Impurity diffusion in pure metals. Part III. Self and impurity diffusion in alloys. Technical report ORNL–3795. USA: Oak Ridge National Laboratory. 78 p.

Atkinson, J.D. & Forrest, J.E. 1985. Factors influencing the rate of growth or fatigue cracks in RPV steels exposed to a simulated PWR primary water environment. Corrosion Science. Vol. 25:8-9. pp. 607-663.

Atkinson, J.D. & Yu, J. 1997. The role of dynamic strain-ageing in the environment assisted cracking observed in pressure vessel steels. Fatigue & Fracture of Engineering Materials & Structures. Vol. 20:1. pp.1-12.

Baird, J.D. 1973. Dynamic strain aging. In: The Inhomogeneity of Plastic Deformation. American Society of Metals, Metals Park, OH, USA. pp. 191 – 222.

Bergström, Y. & Roberts, W. 1971. The application of a dislocation model to dynamical strain ageing in α-iron containing interstitial atoms. Acta Metallurgica. Vol. 19:8. pp. 815-823.

Blanter, M.S., Golovin, I.S., Neuhäuser, H. & Sinning, H.R. 2007. Internal friction in metallic materials. In: Hull, R., Osgood, Jr., R.M, Parisi, J. & Warlimont, H. (eds.) Springer Series in Materials Science, Vol. 90. Verlag Berlin Heidelberg: Springer. 539 p.

Bolling, G.F. & Richman, R.H. 1965. Continual mechanical twinning: Part I: Formal description. Acta Metallurgica. Vol. 13:7. pp. 709-722.

Bolling, G.F. & Richman, R.H. 1965. Continual mechanical twinning: Part II : Standard Experiments. Acta Metallurgica. Vol. 13:7. pp. 723-743.

Bolling, G.F. & Richman, R.H. 1965. Continual mechanical twinning: Part III: Nucleation and dislocation production. Part IV: Cyclic twinning in Fe3Be single crystals. Acta Metallurgica. Vol. 13:7. pp. 745-757.

Brzeski, J.M., Hack, J.E., Darolia, R. & Field, R.D. 1993. Strain aging embrittlement of the ordered intermetallic compound NiAl. Materials Science and Engineering: A. Vol. 170:1-2. pp. 11-18.

Burdett, C. F. & Queen, T. J. 1970. The role of dislocations in damping. International Materials Reviews, Vol. 15:1. pp. 47-85

Chen, W. & Chaturvedi, M.C. 1997. On the mechanism of serrated deformation in aged Inconel 718. Materials Science and Engineering A. Vol. 229:1-2. pp. 163-168.

Clough, W.R., Jackman, L. & Andreev, Y.G. 1968. Dynamic strain aging and the Charpy specimen behaviour of annealed 4340 steel. Transactions of the ASME. Series D, Journal of Basic Engineering. Vol. 90. pp. 13-20.

Cottrell, A.H. & Bilby, B.A. 1949. Dislocation theory of yielding and strain ageing of Iron. Proceedings of Physical Society A. Vol. 62:1. pp. 49-62.

Cottrell, A.H. 1953. LXXXVI. A note on the Portevin-Le Chatelier effect. Philosophical Magazine Series 7. Vol. 44:355. pp. 829-832.

de Almeida, L.H., Emygdio, P.R.O. & Le May, I. 1994. Activation energy calculation and dynamic strain aging in austenitic stainless steel. Scripta Metallurgica et Materialia. Vol. 31:5. pp. 505-510.

de Almeida, L.H., Le May I. & Emygdio, P.R.O. 1998. Mechanistic modelling of dynamic strain aging in austenitic stainless steels. Materials Characterization. Vol. 41:4. pp. 137-150.

Ehrnstén, U., Aaltonen, P., Nenonen, P., Hänninen, H., Jansson, C. & Angeliu, T. 2001. Intergranular cracking of AISI 316NG stainless steel in BWR environment. Proceedings of 10th International Conference on Environmental Degradation of Materials in Nuclear Power Systems - Water Reactors. Nevada, USA, 5 – 9 August, ANS; NACE; TMS (2001), 10 p.

Ehrnstén U., Toivonen A., Ivanchenko M., Nevdacha V., Yagodzinskyy Y. & Hänninen H. 2007. Dynamic strain ageing of deformed nitrogen-alloyed AISI 316 stainless steels. In: Feron D. & Olive J.-M. (eds.) Corrosion Issues in Light Water Reactors. Cambridge, England: Woodhead Publishing, 2007. pp. 103-118.

Friedel, J. 1964. Dislocations. Oxford, United Kingdom: Pergamon Press. 491 p.

Fournier, L., Delafosse, D., Magnin, T. 2001. Oxidation induced intergranular cracking and Portevin – Le Chatelier effect in nickel base superalloy 718. Materials Science and Engineering A. Vol. 316. pp. 166 – 173.

Ganesan, V., Mathew, M.D. & Sankara Rao, K.B. 2009. Influence of nitrogen on tensile properties of 316LN SS. Materials Science and Technology, Vol. 25:5. pp. 614-618.

Gopinath, K., Gogia, A.K., Kamat, S.V. & Ramamurty, U. 2009. Dynamic strain ageing in Ni-base superalloy 720Li. Acta Materialia. Vol. 57:4. pp. 1243-1253.

Grujicic, M., Nilsson, J.-O., Owen, W.S. & Thorvaldsson, T. 1988. Basic deformation mechanisms in nitrogen strengthened stable austenitic stainless steels. In: Foct, J. & Hendry, A. (eds.) Proceedings of the International Conference on High Nitrogen Steels '88. Lille, France. 18-20.5.1988. London: The Institute of Metals, 1989. pp. 151-158.

Grujicic, M. & Owen, W. 1995. Models of short-range order in a face-centered cubic Fe-Ni-Cr alloy with a high concentration of nitrogen. Acta Metallurgica et Materialia. Vol. 43:11. pp. 4201-4211.

Hale, C.L., Rollings, W.S. & Weaver, M.L. 2001. Activation energy calculations for discontinuous yielding in Inconel 718SPF. Materials Science and Engineering A. Vol. 300:1-2. pp. 153-164.

Hayes, R.W. 1983. On a proposed theory for the disappearance of serrated flow in f.c.c. Ni alloys. Acta Metallurgica. Vol. 31:3. pp. 365-371.

Hayes, R.W. & Hayes, W.C. 1982. On the mechanism of delayed discontinuous plastic flow in an age-hardened nickel alloy. Acta Metallurgica. Vol. 30:7. pp. 1295-1301.

Hasiguti, R.R., Igata, N. & Kamoshita, G. 1962. Internal friction peaks in cold-worked metals. Acta Metallurgica. Vol. 10:4. pp. 442-447.

Hong, S.H., Kim, H.Y., Jang, J.S. & Kuk, I.H. 1996. Dynamic strain aging behavior of Inconel 600 alloy. In: R. D. Kissinger, et al (eds.) Superalloys 1996. Champion, Pennsylvania, USA. 22–26.09.1996. TMS, 1996. pp. 401-407.

Hong, S. & Lee, S. 2005a. Mechanism of dynamic strain aging and characterization of its effect on the low-cycle fatigue behavior in type 316L stainless steel. Journal of Nuclear Materials. Vol. 340:2-3. pp. 307-314.

Hong, S., Lee, K. & Lee, S. 2005b. Dynamic strain aging effect on the fatigue resistance of type 316L stainless steel. International Journal of Fatigue. Vol. 27:10-12. pp. 1420-1424.

Hong, S. & Lee, S. 2004a. Dynamic strain aging under tensile and LCF loading conditions, and their comparison in cold worked 316L stainless steel. Journal of Nuclear Materials. Vol. 328:2-3. pp. 232-242.

Hong, S. & Lee, S. 2004b. The tensile and low-cycle fatigue behavior of cold worked 316L stainless steel: influence of dynamic strain aging. International Journal of Fatigue. Vol. 26:8. pp. 899-910.

Hänninen, H., Aaltonen, P., Brederholm, A., Ehrnstén, U., Gripenberg, H., Toivonen, A., Pitkänen, J. & Virkkunen, I. 2006. Dissimilar metal weld joints and their performance in nuclear power plant and oil refinery conditions. VTT – Research Notes 2347. VTT 2006. 208 p.

Hänninen, H., Seifert, H.P., Yagodzinskyy, Y., Ehrnstén, U., Tarasenko, O. & Aaltonen P. 2001. Effects of dynamic strain ageing on environment-assisted cracking of low alloy pressure vessel and piping steels. Proceedings of the 10th International Conference on Environmental Degradation of Materials in Nuclear Power Systems – Water Reactors. Lake Tahoe, Nevada, USA. 6-10.8.2001. NACE/TMS/ANS, 2001. (CDROM) Paper No. 47.

Ismail, M.I., Iskander, S.S. & Saleh, E.B. 1981. Carburizing of steels. Surface Technology. Vol. 12:4. pp. 341-349.

Ivanchenko, M., Yagodzinskyy, Y., Ehrnsten, U., Karlsen, W. & Hänninen, H. 2009. Manifestation of DSA in austenitic stainless steel and Inconel alloys. Proceedings of the 20th International Conference on Structural Mechanics in Reactor Technology (SMiRT 20). Espoo, Finland. 9-14.8.2009. (CDROM). Paper No. 2013.

Iwamoto, M. & Fukai, Y. 1999. Superabundant vacancy formation in iron under high hydrogen pressures: Thermal desorption spectroscopy. Materials Transactions JIM. Vol. 40:7. pp. 606-611.

Jagodzinski, Yu., Smouk, S., Tarasenko, A. & Hänninen, H. 1998. Distribution of interstitial impurities and their diffusion parameters in high-nitrogen steels studied by means of internal friction. In: Hänninen, H., Hertzman, S. & Romu, J. (eds.) Proceedings of the 5th International Conference on High Nitrogen Steels ’98. Espoo, Finland. 24-26.5.1998. Stockholm, Sweden. 27-28.5.1998. Switzerland: Trans Tech Publication Ltd, 1999. pp. 47-52.

James, L.A. & Porr, W.C. 1999. The effect of an elevated temperature aqueous environment upon the J-controlled tearing of a low-alloy steel. International Journal of Pressure Vessels and Piping. Vol. 76:11. pp. 769-779.

Jenkins, C.F. & Smith, G.V. 1969. Serrated plastic flow in austenitic stainless steel. Transactions of the Metallurgical Society of AIME. Vol. 245. pp. 2149-2156.

Kang, S. S. & Kim, I. S. 1992. Dynamic strain-aging effect on fracture toughness of vessel steels. Nuclear Technol. Vol. 97. pp. 336-343.

Katada, Y. & Nagata, N. 1985. The effect of temperature on fatigue crack growth behaviour of a low alloy pressure vessel steel in a simulated BWR environment Corrosion Science. Vol. 25:8-9. pp. 693 - 704.

Keh, A. S., Nakada, Y. & Leslie W. C. 1968. Dynamic strain-aging in iron and steels. In: Rosenfield A.R. (Ed.). Dislocation Dynamics. New York, USA: McGraw-Hill, 1968. pp. 381 – 408.

Kikuta, Y., Araki, T. & Yoneda M. 1982. Hydrogen embrittlement and dynamic strain ageing in steel at elevated temperature. Proceeding of the Third International Congress on Hydrogen and Materials. Paris, France, 7–11.1982. pp. 599-604.

Kim, I.S. & Kang, S.S. 1995. Dynamic strain aging in SA508-class 3 pressure vessel steel. International Journal of Pressure Vessels & Piping. Vol. 62:2. pp. 123-129.

Kim, D.W., Ryu, W.-S., Hong, J.H. & Choi, S.-K. 1998. Effect of nitrogen on the dynamic strain aging behaviour of type 316L stainless steel. Journal of Material Science. Vol. 33:3. pp. 675 – 679.

Kimura, A. & Birnbaum, H.K. 1990. Anomalous strain rate dependence of the serrated flow in Ni-H and Ni-C-H alloys. Acta Metallurgica et Materialia. Vol. 38:7. pp. 1343-1348.

Kocks, U.F., Cook, R.E. & Mulford, R.A. 1985. Strain aging and strain hardening in Ni-C alloys. Acta Metallurgica. Vol. 33:4. pp. 623-638.

Kohandehghan, A.R., Sadeghi, A.R., Akhgar, J.M. & Serajzadeh, S. 2010. Investigation into dynamic strain aging behaviour in high carbon steel. Ironmaking and Steelmaking. Vol. 37:2. pp. 155-160.

Korbel, A., Zasadzinski, J. & Sieklucka, Z. 1976. A new approach to the Portevin-Le Chatelier effect. Acta Metall. Vol. 24. pp. 919 – 923.

Lai, J.K.L. 1983. A study of precipitation in AISI type 316 stainless steel. Materials Science and Engineering. Vol. 58:2. pp. 195-209.

Li, C.-C. & Leslie, W.C. 1978. Effects of dynamic strain aging on the subsequent mechanical properties of carbon steels. Metallurgical Transactions A. Vol. 9:12. pp. 1765-1775.

Mannan, S.L., Samuel, K.G. & Rodriguez, P. 1983. Dynamic strain ageing in type 316 stainless steel. Transactions of the Indian Institute of Metals. Vol. 36:4-5. pp. 313 – 320.

McCormick, P.G. 1972. A model for the Portevin-Le Chatelier effect in substitutional alloys. Acta Metallurgica. Vol. 20. pp. 351 – 354.

McCormick, P.G. 1988. Theory of flow localisation due to dynamic strain ageing. Acta Metallurgica. Vol. 36:12. pp. 3061-3067.

Mesarovic, S.Dj. 1995. Dynamic strain aging and plastic instabilities. Journal of the Mechanics and Physics of Solids. Vol. 43:5. pp. 671 – 700.

Mohan, R. & Marschall, C. 1998. Cracking instabilities in a low-carbon steel susceptible to dynamic strain aging. Acta Materialia. Vol. 46:6. pp. 1933 – 1948.

Mulford R.A. & Kocks U.F. 1979. New observations on the mechanisms of dynamic strain aging and of jerky flow. Acta Metallurgica. Vol. 27:7. pp. 1125-1134.

Nagumo, M., Yagi, T. & Saitoh, H. 2000. Deformation-induced defects controlling fracture toughness of steel revealed by tritium desorption behaviours. Acta Materialia. Vol. 48. pp. 943-951.

Nakada, Y. & Keh, A.S. 1970. Serrated flow in Ni-C alloys. Acta Metallurgica. Vol. 18:4. pp. 437-443.

Nowick, A.S. & Berry, B.S. 1972. Anelastic relaxation in crystalline solids. N.Y., USA and London, United Kingdom: Academic Press. 677 p.

Oriani, R.A. 1972. A mechanistic theory of hydrogen embrittlement of steels. Berichte der Bunsen-Gesellschaft für Physikalische Chemie. Vol. 76:8. pp. 848-857.

Penning, P. 1972. Mathematics of the Portevin-le Chatelier effect. Acta Metallurgica. Vol. 20:10. pp. 1169-1175.

Portevin, A. & Le Chatelier, F. 1923. Sur un phénomène observé lors de l'essai de traction d'alliages en cours de transformation. Comptes Rendus de l'Academie des Sciences, Paris. Vol. 176. pp. 507-510.

Rao, K.B.S., Kalluri, S., Halford, G.R. & McGaw, M.A. 1995. Serrated flow and deformation substructure at room temperature in Inconel 718 superalloy during strain controlled fatigue. Scripta Metallurgica et Materialia. Vol. 32:4. pp. 493-498.

Roberts M.J. & Owen W.S. 1970. Unstable flow in martensite and ferrite. Metallurgical Transactions. Vol:1. pp. 3203-3213.

Rodriguez P. 1984. Serrated plastic flow. Bulletin of Materials Science. Vol. 6:4. pp. 653-663.

Rose, K.S.B. & Glover, S.G. 1966. A study of strain-ageing in austenite. Acta Metallurgica. Vol. 14:11. pp. 1505-1516.

Rosin K.M. & Finkelshtein B.N. 1953. A study of phase transformations by the method of internal friction. Doklady Akademii Nauk SSSR. Vol. 91:4. pp. 811-814.

Samuel, E.I., Choudhary, B.K. & Bhanu Sankara Rao, K. 2002. Influence of temperature and strain rate on tensile work hardening behaviour of type 316 LN austenitic stainless steel. Scripta Materialia, Vol. 46: 7. pp. 507-512.

Samuel, K.G., Mannan, S.L. & Rodriguez, P. 1988. Serrated yielding in AISI 316 stainless steel. Acta Metallurgica, Vol. 36: 8. pp. 2323-2327.

Seifert, H.P. & Ritter S. 2002. Environmentally-assisted cracking of low-alloy reactor pressure vessel steels under boiling water reactor conditions. Paul Scherrer Institute Reports 2002. PSI-BERICHT-02-05. 119 p.

Shi, L. & Northwood, D.O. 1995. The mechanical behavior of an AISI type 310 stainless steel. Acta Metallurgica et Materialia. Vol. 43:2. pp. 453-460.

Schwarz, R.B. & Funk, L.L. 1985. Kinetics of Portevin-Le Chatelier effect in Al 6061 alloy. Acta Metall. Vol. 33. pp. 295–307.

Schoeck, G. & Seeger, A. 1959. The flow stress of iron and its dependence on impurities. Acta Metallurgica. Vol. 7:7. pp. 469-477.

Snoek, J. L. 1941. On the decarburization of steel and related questions. Physica. Vol. 8. pp. 734–744

van den Beukel, A. 1975. Theory of the effect of dynamic strain aging on mechanical properties. Physica Status Solidi A. Vol. 80. pp. 197-206.

Venkadesan, S., Phaniraj, C., Sivaprasad, P.V. & Rodriguez, P. 1992. Activation energy for serrated flow in a 15Cr − 5Ni Ti-modified austenitic stainless steel. Acta Metallurgica et Materialia. Vol. 40:3. pp. 569-580.

Verner V.D. 1965. Nature of the internal friction peak in face-centered cubic interstitial solid solutions. Soviet Physics – Solid State (USA). Vol. 7:8. pp. 1874-1880.

Yagodzinskyy Y., Andronova E., Ivanchenko M. & Hänninen H. 2009. Anelastic mechanical loss spectrometry of hydrogen in austenitic stainless steels. Materials Science and Engineering A. Vol. 521-522. pp. 159-162.

ISBN 978-952-60-3444-7
ISBN 978-952-60-3445-4 (PDF)
ISSN 1795-2239
ISSN 1795-4584 (PDF)